Mechanical and physical behavior of high-porosity chalks exposed to chemical perturbation

M. Megawati, M. V. Madland, A. Hiort

Abstract

Extensive study on the effect of dissolution–precipitation on mechanical behavior of various high-porosity outcrop chalks (Liége, Aalborg, Kansas, Stevns Klint, and Mons) flooded with simplified aqueous chemistry at 130 °C under isotropic stress beyond the yield is performed. Chemical effects induced by injection of 0.219 M $MgCl_2$ solutions into impure chalks (Liége, Aalborg, Kansas) lead to an immediate enhancement on the macroscopic creep with more than a factor of 2 larger than that of exposed to 0.657 M NaCl solutions. In pure chalks (Stevns Klint and Mons) however, the creep response is characterized by a time lag, where creep initially diminishes before a tertiary-like creep develops. Systematic correlation between calcite dissolution and the resulting creep strain is consistently demonstrated by all the different chalk types.

The chemical effects are described as precipitation of Mg-bearing minerals and dissolution processes, which involve both the carbonate and non-carbonate phases. SEM-EDS, XRD, and BET (N_2) analyses indicate newly formed Mg-bearing minerals primarily present as Magnesite, which precipitated in the pore space. Enhanced dissolution is shown by continuous production of Ca^{2+} measured in the core effluent. The time for the dissolution to overcome intergranular friction accounts for the delay in the creep acceleration in pure chalks (Stevns Klint and Mons). For impure chalks (Liége, Aalborg, Kansas) chemical alterations on the non-carbonate phases outweigh the intergranular friction. This additional effect accounts for the immediate impact in the creep deformation.

The chemical effects are also demonstrated by marked reduction in the permeability. The porosity–permeability relationship measured at the end of creep test is shifted down from the initial correlation, indicating a dramatic increase in the chalk specific surface area.

Keywords; Chalk, rock mechanics, chemical effect, dissolution, precipitation, creep, compaction, water weakening, porosity, permeability

1. Introduction

Dissolution and precipitation in porous media have significant implications for petroleum reservoirs not only related to the diagenetic history but also when the field is brought onto production. It is a major mechanism in the pressure solution processes, which have been well-documented in describing sedimentary and fault rock deformation (Durney, 1972; Rutter, 1983; Tada and Siever, 1989; Yasuhara et al., 2005), porosity–permeability evolution (Bjørkum and Nadeau, 1998; Ehrenberg et al., 2006), and development of stylolites in carbonate reservoir (Renard et al., 2004; Laronne Ben-Itzhak et al., 2012). One of the important implications of these processes is the formation of different pressure regimes in North Sea central graben, which impacts fluid pressure release and build-up (Swarbrick and Osborne, 1998).

In the North sea, chalk reservoir compaction and seabed subsidence at the Ekofisk field has been a subject of extensive research. Chemical effects due to reactions between the chalk framework and the injected water are one of the major mechanisms in the so-called water weakening processes (Newman, 1983; Rhett and Teufel, 1991; Teufel and Rhett, 1992; Piau and Maury, 1994; Risnes and Flaageng, 1999; Risnes et al., 2005; Madland et al., 2011). Chemical dissolution precipitation have been investigated through various approaches such as numerical simulations (Pietruszczak et al., 2006; Lydzba et al., 2007; Hu and Hueckel, 2007; Hueckel and Hu, 2007), experimental studies (Hellmann et al., 2002b), as well as microscopic studies (Hellmann et al., 2002a). Despite numerous research, integrated study on direct correlation of dissolution precipitation effects and the mechanical properties are, however, limited.

Pore water chemistry and the presence of clays have been shown to impact the kinetics of dissolution precipitation. It has been generally agreed that the presence of clays promotes pressure solution in chalk. In Baker et al. (1980) the presence of clay is shown to inhibit precipitation of calcite, but does not retard calcite dissolution. Weyl (1959) showed that the presence of thin clay seams facilitates diffusional transport in pressure solution process. Garrison and Kennedy (1977) pointed out that dissolution is most intense in layers that have high primary clay content. Fabricius and Borre (2007) also concluded that the contact between calcite and clay causes a disequilibrium for calcite dissolution.

In terms of chalk mechanical behavior, earlier works (Heggheim et al., 2005; Korsnes et al., 2006a,b; Madland et al., 2011) have shown that not only the aqueous chemistry of the pore fluid, but also the presence of non-carbonate minerals such as silica and clay minerals control the chalk mechanical behavior. In Madland et al. (2011) injecting $MgCl_2$ brine leads to supersaturation of new minerals which further shift the chemical equilibrium towards dissolution of calcite. When injecting NaCl brine with the same ionic strength, however, only a minor change in the aqueous chemistry was demonstrated.

The primary focus of the present study is to link dissolution–precipitation to the mechanical and physical properties of chalk, and to investigate how the variation in chalk mineralogy impacts the chemical and mechanical interactions. Long-term mechanical tests on various outcrop chalks were carried out. Chalk cores were loaded isotropically beyond their yield points and then a prolonged creep phase with continuous injection of different aqueous chemistry followed. Simplified brines with seawater ionic strength (0.219 M $MgCl_2$ and 0.657 M NaCl) were used. Since mechanical properties measured under isotropic compression are less scattered and highly repeatable as shown from previous studies (Risnes et al., 2003; Heggheim et al., 2005; Korsnes et al., 2006b, 2008; Zangiabadi et al., 2009; Madland et al.,

2011), this type of test is chosen. Microscopic studies by Scanning Electron Microscopy (SEM) are included. High-porosity outcrop chalks of different mineralogical compositions and of different origins from Niobrara quarry Kansas US, Aalborg quarry and Stevns Klint Denmark, Liége quarry and Mons basin Belgium were used. These will also serve as a basis for geomechanical characterization of high-porosity outcrop chalks.

2. Materials and Method

2.1. Material properties

We used five different outcrop chalks representing high-porosity chalk with variable properties such as calcite purity, mineralogy, permeability, and specific surface area. The properties of the five chalk types are presented in Table 1. Porosity was calculated from the difference between the dry and wet weight after saturating the core plug with distilled water in a vacuum chamber. Permeability was calculated from the measured pressure drop across the core plug where a constant rate was applied. Carbonate content was measured by 0.5 M NaOH titration after reacting approximately 0.3 g chalk powder with an excess of 0.5 M HCl. The accuracy of this method for chalk is 0.7% or better (Nguyen, 2008). Specific surface area (SSA) on bulk chalk sample was measured by BET (N_2) method in two different Labs using Coulter SA3100 and Micromeritics Gemini III 2375.

Table 1. Physical properties of different chalk types used in the study. The number of samples measured for SSA is shown in the parantheses. Grain density for all the chalk types is 2.7 g/cm^3.

Chalk type	**Age**	**ϕ (%)**	**κ (mD)**	**Carbonate content (%)**	**SSA (m^2/g)**
Stevns Klint (SK)	Maastrichtian	43–47	3–5	99.66	$1.89_{(2)}$
Aalborg (ÅR)	Maastrichtian	45–48	3–5	95.61	$2.45_{(3)}$
Liége (RL)	Campanian	40–42	1–2	94.84	$3.90_{(4)}$
Mons (MO)	Campanian	42–44	3–5	99.7	$1.81_{(3)}$
Kansas (KA)	Late Cretaceous	37–40	1–2	97.20	$2.95_{(2)}$

2.2. Rock mechanical test procedure

Rock mechanical testing was performed in a hydraulically operated triaxial cell similar with that of previous studies (Risnes et al., 2005; Korsnes et al., 2008; Madland et al., 2011). The aim has thus not been to capture strength variations from complete yield curves, but to select a repeatable test method in order to study the various chemical effects. The design of the Triaxial cell is such that the application of confining pressure is also compensated in the axial direction. Confining pressure and axial pressure were applied using hydraulic high pressure pumps. The cell is equipped with a heating jacket element with an external regulator system. The test temperature was set to 130 °C.

Vertical displacement was measured continuously using an LVDT (Low Voltage Displacement Transducer) with a resolution of 0.05 mm or better. For total strain calculation, displacement at the start of the isotropic loading was taken as a reference point.

Prior to mechanical testing, a core plug with a size 38.1 mm diameter and 70 mm long was firstly cleaned by flushing through 2 pore volumes (PV's) of Distilled Water (DW) with 0.5 MPa isotropic pressures. Differential pressure across the core was measured, and during the cleaning initial permeability was calculated (Table 1). After cleaning, pore pressure in the back side and confining pressure were simultaneously increased to 0.7 MPa and 1.2 MPa respectively. Thereafter, heating elements jacketing the Triaxial cell were switched on and the temperature was increased to 130 °C. The temperature is kept constant (±0.2 °C) throughout

the test by an external regulating system. When the temperature is stable at 130 °C, the respective brine was introduced and the system was then left to equilibrate overnight.

All the tests were performed isotropically beyond yield point, and then followed by a prolonged creep phase. The loading rates are about 0.2 and 0.3 bar/min for SK/MO/RL/ÅR chalks and KA chalk, respectively. Throughout the tests, brine was continuously injected with a fixed rate of 1 PV/day. The brine composition and initial pH are presented in Table 2. Effluent was collected periodically at the core exit and analyzed off-line by an Ion-Exchange Chromatograph (ICS-3000 Dionex) in attempt to study any chemical changes in and out of the core.

Table 2. Brine composition injected during mechanical tests.

Ions	**0.657 M NaCl (mol/l)**	**0.219 M $MgCl_2$ (mol/l)**
Cl^-	0.657	0.438
Mg^{2+}	0.000	0.219
Ca^{2+}	0.000	0.000
Na^+	0.657	0.000
Ionic strength	0.657	0.657
TDS (g/l)	38.40	20.84
pH	6.12	5.62

2.3. Time-dependent creep

Extensive creep tests were performed during a period ranging from 10 days to more than 300 days. Creep stress level is kept similar within the same chalk type. Total isotropic stress was approximately 12, 11, 11, 11, and 19 MPa for Mons, Stevns Klint, Aalborg, Liége, and Kansas, respectively.

Rate-type creep model (Andersen et al., 1992), which is a well-known method for modeling of North sea chalk, is adopted here to model creep behavior over time. The simplified rate-type model with parameter A and t_0 can be expressed as follows:

$$(1)\ \varepsilon_{creep} = A \ln(1 + t/t_0)$$

Parameter A and t_0 are related to the compressibility and consolidation time, respectively, described in more detail in Andersen et al. (1992). Here, the values were calculated from the best-fit to the measured creep.

Real-time axial displacement was continuously measured, from which deformation was calculated. Creep rate is obtained from the derivative of the measured creep with time as follows:

$$(2)\quad \dot{\varepsilon} = \frac{dl/dt}{l_0}$$

where dl and l_0 are the displacement and the original dimension of the core, respectively. For infinite time, the rate type model predicts a diminishing creep, where the rate converges to zero. A comparison between the measured creep rate data and the model were performed and

any deviation will thus represent the measurable effect of chemical processes on the time-dependent deformation.

3. Results

3.1. Stevns Klint (SK)

The SK chalk can be classified as an extremely pure coccolith mudstone (Hjuler, 2007) with more than 99% calcite content (Table 3).

Table 3. Mechanical test results of Stevns Klint (SK) chalk based on isotropic compression in Fig. 1.

Core ID	Por. (%)	Fluid	Yield point (MPa)	Bulk modulus (GPa)
SK15	44.99	0.219 M $MgCl_2$	8.3	0.72
SK36B	44.42	0.219 M $MgCl_2$	7.4	0.65
SK5	45.71	0.219 M $MgCl_2$	7.6	0.74
SK4	45.40	0.657 M NaCl	7.6	0.72
SK23	45.41	0.657 M NaCl	7.4	0.64
SK36	45.03	DW	8.5	0.59

Stress versus strain during isotropic loading phase for all SK core plugs tested is shown in Fig. 1. Injections of different aqueous chemistry (0.657 M NaCl or 0.219 M $MgCl_2$) do not seem to give clear effect on the yield point and bulk modulus of SK cores. The yield points are within 8 MPa and the bulk moduli are in the range of 0.6–0.7 GPa. Core plug SK36 flooded with DW for example exhibits quite similar behavior as those flooded with saline brines.

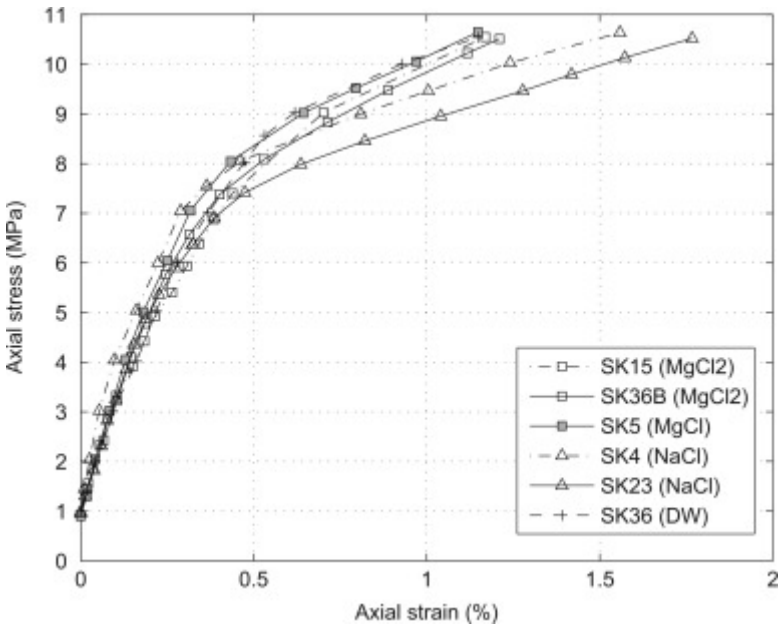

Fig. 1. Axial stress versus axial strain of SK cores flooded with 0.657 M NaCl and 0.219 M $MgCl_2$ at 130 °C.

While no systematic trend is demonstrated in the loading phase, creep development with time does demonstrate a clear influence of the aqueous chemistry injected (Fig. 2). Cores flooded with 0.657 M NaCl follow a similar trend as that of DW. Both show a larger creep deformation which develops with decreasing rate with time. Creep strain for cores flooded with 0.219 M $MgCl_2$ on the other hand flattens out after the primary phase. The creep is diminishing and after around 10 h it nearly stops. In the time frame of the test period SK15 and SK36B the total creep are significantly smaller than that of NaCl or DW flooding. However, as the creep test is allowed to prolong, as shown by SK5, another phase which appears as a tertiary creep develops after approximately 150 h. The creep rate accelerates by a magnitude higher and exceeds that of NaCl or DW flooding. Over a longer time period the creep strain will apparently exceed that of DW and NaCl.

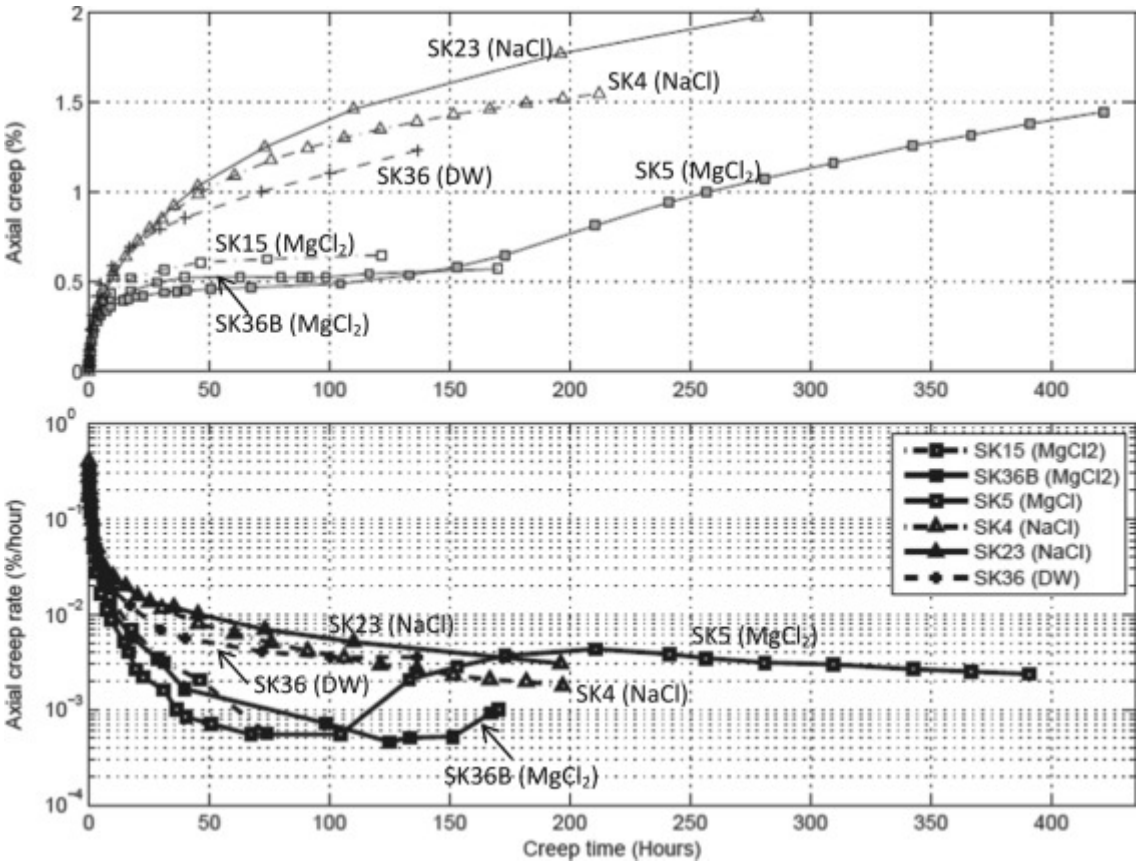

Fig. 2. Axial creep strain (upper) and creep rate (lower) with time of SK cores flooded with 0.657 M NaCl and 0.219 M $MgCl_2$ at 130 °C. Cores flooded with DW and 0.657 M NaCl unexpectedly develop larger strain but the rates are declining with time. Cores flooded with 0.219 M $MgCl_2$ initially experience a creep diminution but thereafter as shown by SK5 a tertiary creep develops with increased creep rate of a magnitude times higher.

Fig. 3 presents the IC analyses of fractioned effluent core SK5 flooded with 0.219 M $MgCl_2$ solution. The results are in agreement with previous work (Madland et al., 2011), which show significant loss of magnesium while in the same time significant production of calcium is

measured. Chloride, however, immediately reaches the original concentration and no specific changes are observed. With total sites of 5 sites/nm2, such Mg^{2+} loss and Ca^{2+} production are in a magnitude too high to result from Ca–Mg substitution alone. In earlier studies (Madland et al., 2011; Megawati et al., 2011), this is instead described as enhanced dissolution. Effluent pH is relatively stable in the range of 7–8. The results also show that the sum of magnesium and calcium concentration is equivalent with the original magnesium concentration.

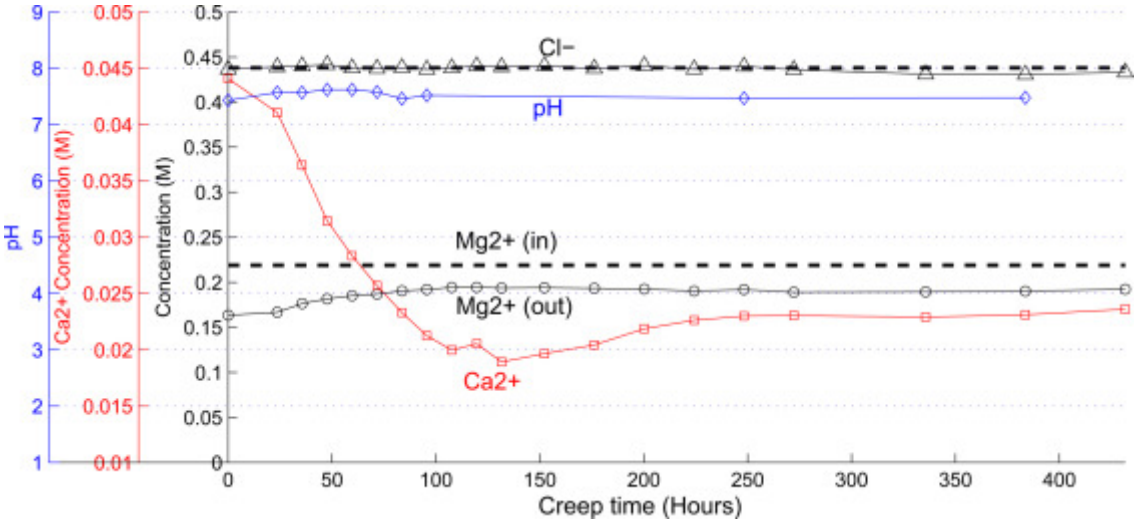

Fig. 3. Mg^{2+}, Ca^{2+}, Cl^{-} concentrations and pH in sampled effluents from core SK5, flooded with 0.219 M $MgCl_2$. Original Mg^{2+} and Cl^{-} concentrations are shown by the dashed lines. Note loss of Mg^{2+} and production of Ca^{2+}, and note increase of Ca^{2+} which coincides with the onset of creep acceleration in Fig. 2.

With fresh brine being continuously injected, the loss of Mg^{2+} and the production of Ca^{2+} are maintained. It is interesting to note that the onset of creep acceleration coincides with significant increase in the Ca^{2+} production of more than 50% after 150-h creep (see Figs. 2 and 3). This points towards a link between dissolution and time-dependent deformation.

For chalk cores flooded with 0.657 M NaCl solution, only minor dissolution is observed. Concentrations of Na^{+} and Cl^{-} are within the original concentration injected as shown in Fig. 4.

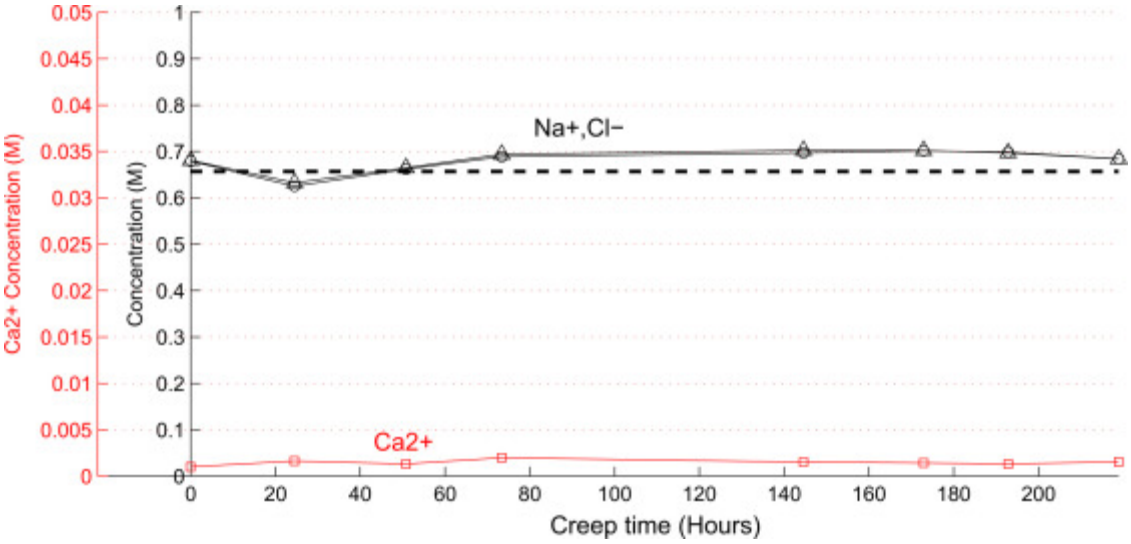

Fig. 4. Na^+, Ca^{2+}, and Cl^- concentrations in sampled effluents from core SK4, flooded with 0.657 M NaCl. Note no change in the Na^+ and only minor production of Ca^{2+}.

Significant dissolution induced by injection of 0.219 M $MgCl_2$ relative to that of 0.657 M NaCl occurs from initial time. It is interesting to note that such dissolution does not immediately impact the macroscopic creep of SK cores. Instead, creep initially stops before a creep enhancement evolves. As shown by extended creep test SK5, creep acceleration and enhanced dissolution occur simultaneously. As the mechanical and the chemical responses are aligned in time, this would mean that the deformation is a chemically triggered mechanism. As creep acceleration is delayed, this would reasonably imply a period of time required for the chemical processes on the grain scale to result in macroscopic mechanical degradation.

3.2. Mons (MO)

Similar as SK chalk, MO chalk is also pure chalk with calcite content more than 99% and can be classified as a coccolith mudstone (Hjuler, 2007).

Stress versus strain in Fig. 5 shows no obvious effect of the aqueous chemistry during the isotropic loading. Sample MO2 experiences high strain upon being loaded above the yield point. Coincidentally the sample has also the highest porosity (Table 4). Variation in the bulk modulus and yield values, summarized in Table 4, seems to rather follow the porosity variation. No clear trend according to the injected fluid is demonstrated.

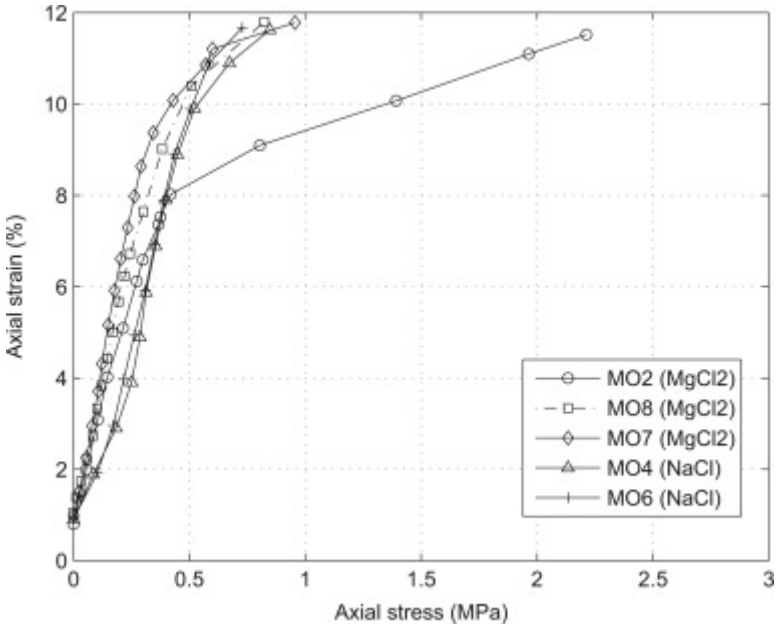

Fig. 5. Axial stress versus axial strain of Mons (MO) cores flooded with 0.657 M NaCl and 0.219 M $MgCl_2$ at 130 °C.

Table 4. Mechanical test results of Mons (MO) chalk based on isotropic compression in Fig. 5.

Core ID	**Por. (%)**	**Fluid**	**Yield point (MPa)**	**Bulk modulus (GPa)**
MO2	43.95	0.219 M $MgCl_2$	8.3	0.62
MO8	42.90	0.219 M $MgCl_2$	10.2	0.79
MO7	43.60	0.219 M $MgCl_2$	9.4	0.97
MO4	43.30	0.657 M NaCl	9.4	0.80
MO6	43	0.657 M NaCl	10.2	0.77

In Figs. 6 and 7 creep strain and rates for Mons Chalk flooded with different fluids are presented. A similar trend with that of Stevns Klint is remarkably shown. Cores exposed to 0.657 M NaCl experience the largest creep deformation but the rates are decreasing with time. Creep curves of those flooded with 0.219 M $MgCl_2$ on the other hand are diminishing and flattening out after around 10 h. Within the time frame of the test periods of sample MO4 and MO6, no further creep develops. However, when the creep test is allowed to run sufficiently long as shown by MO2, an acceleration stage develops after approximately 300 h-creep. Creep rate increases by several orders of magnitude, exceeding that of NaCl flooding. This clearly shows that the time period is substantial.

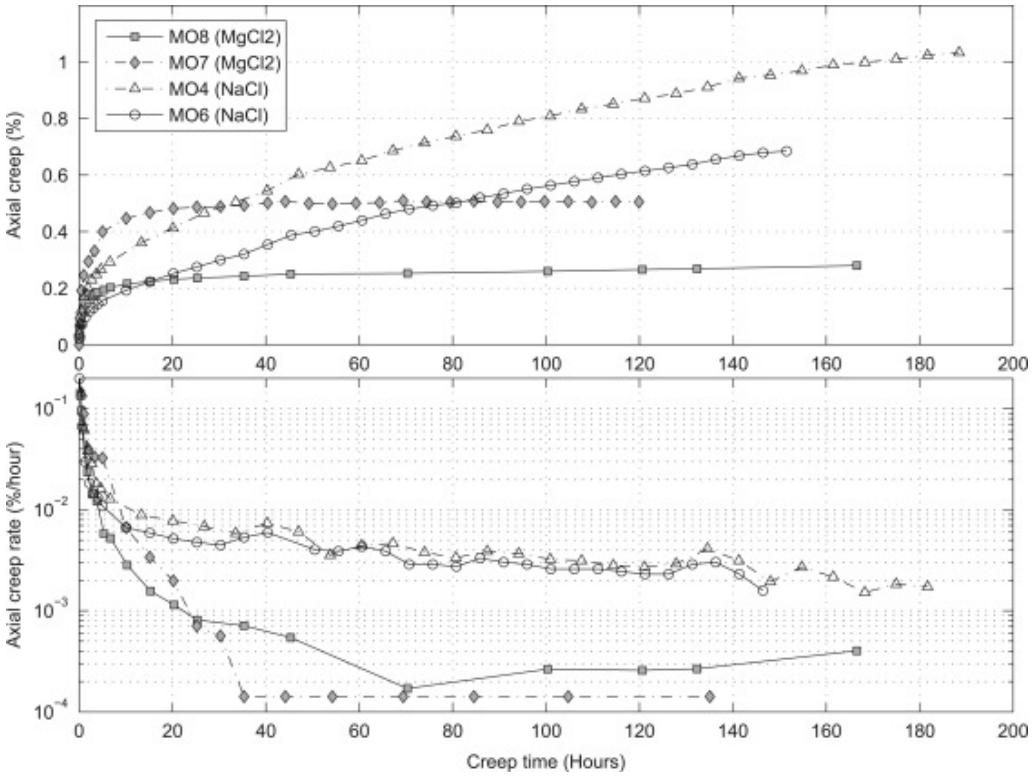

Fig. 6. Axial creep strain (upper) and creep rate (lower) with time of MO cores flooded with 0.657 M NaCl and 0.219 M $MgCl_2$ at 130 °C. Cores flooded with 0.657 M NaCl unexpectedly develop larger strain. Cores flooded with 0.219 M $MgCl_2$, however, experience a creep diminution within the 180-h creep period.

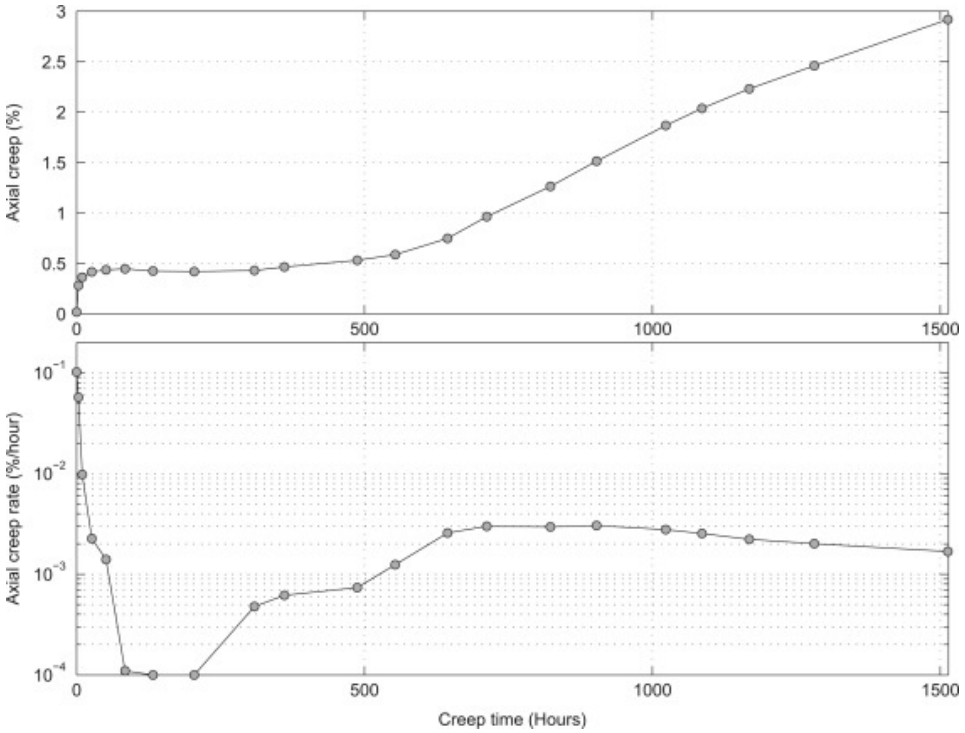

Fig. 7. Axial creep strain (upper) and creep rate (lower) with time of MO2 core flooded with 0.219 M $MgCl_2$ at 130 °C, prolonged creep phase of more than 1500 h. Tertiary creep-like evolves approximately after 300 h where the rate is increased by a magnitude higher.

Chemical analysis on the effluent of MO chalks flooded with 0.219 M $MgCl_2$ shows continuous loss of Magnesium and at the same time production of Calcium is measured (Fig. 8). For cores flooded with 0.657 M NaCl only minor production of calcium and relatively no change in the Na^+ is shown (Fig. 9). Chemical analysis on extended test core MO2 shows that, after approximately 300 h, a marked increase in the Ca^{2+} production is demonstrated. Similar to that observed in SK chalk, such onset in the enhanced dissolution is also followed by acceleration in the creep deformation (Fig. 7). No marked change, however, is observed in the Mg^{2+} concentration. This shows that the triggering mechanisms must be related to dissolution.

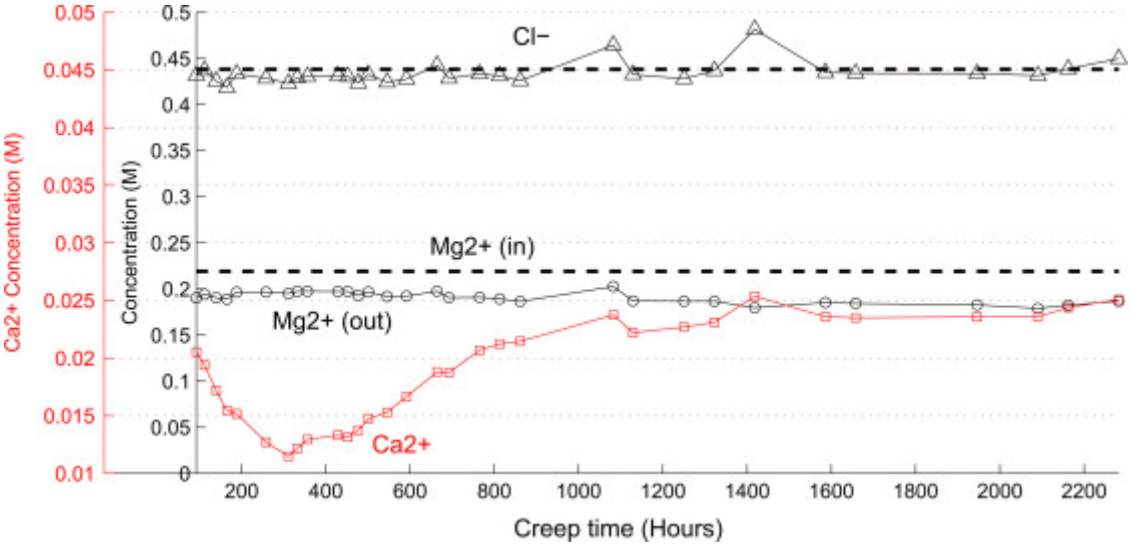

Fig. 8. Mg^{2+}, Ca^{2+}, and Cl^- concentrations in sampled effluents from core MO2, flooded with 0.219 M $MgCl_2$. Original Mg^{2+} and Cl^- concentrations are shown by dashed line. Note loss of Mg^{2+} and production of Ca^{2+} and note increase of Ca^{2+} which coincides with the onset of creep acceleration in Fig. 7.

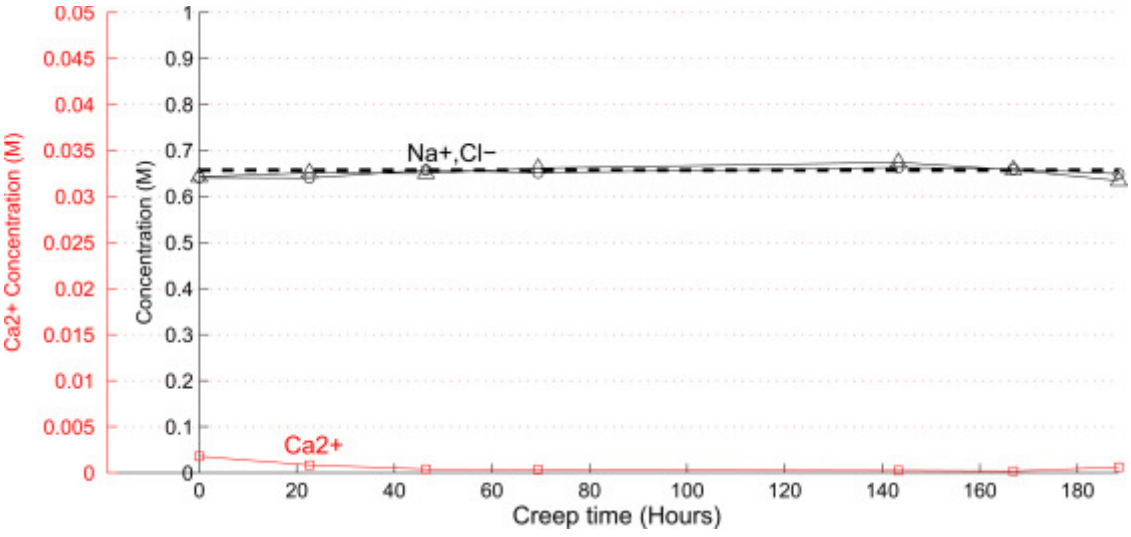

Fig. 9. Na^+, Ca^{2+}, and Cl^- concentrations in sampled effluents from core MO4, flooded with 0.657 M NaCl. No change in the Na^+ and only minor production of Ca^{2+}.

3.3. Kansas (KA)

KA chalk is rather impure with calcite content of about 97% and it can be classified as coccolith mudstone or wackestone (Hjuler and Fabricius, 2009). Cementation and recrystallization are common in KA chalk, resulting in rather angular grain shapes.

Stress versus strain during isotropic loading (Fig. 10) trend towards lower bulk modulus for all the $MgCl_2$ flooded-cores. Yield point and bulk modulus are lower than that of NaCl flooding. Concurrently the porosity is also relatively higher than those of NaCl-flooded and hence it may also influence the stress–strain behavior (Table 5).

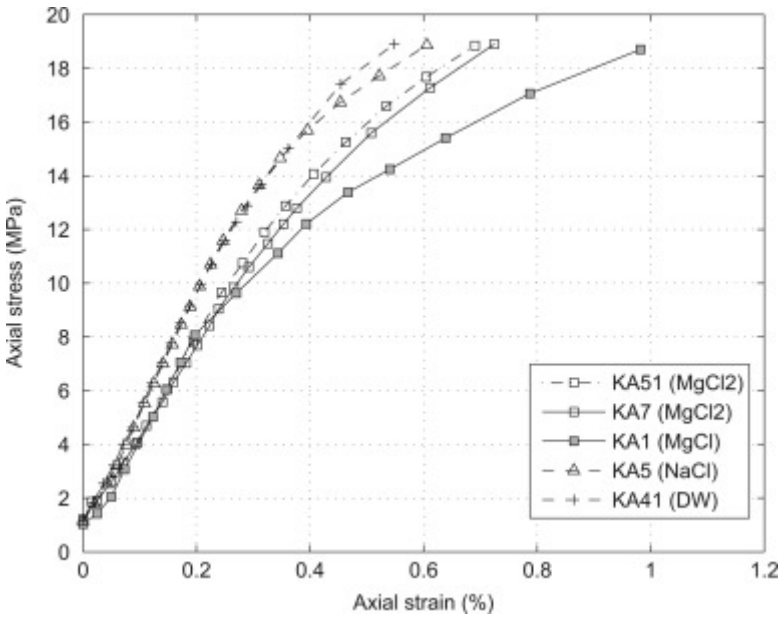

Fig. 10. Axial stress versus axial strain of Kansas (KA) cores flooded with 0.657 M NaCl and 0.219 M $MgCl_{2+}$ at 130 °C. Note KA1 has the highest porosity.

Table 5. Mechanical test results of Kansas (KA) chalk based on isotropic compression in Fig. 10.

Core ID	**Por. (%)**	**Fluid**	**Yield point (MPa)**	**Bulk modulus (GPa)**
KA51	38.63	0.219 M $MgCl_2$	14.1	1.21
KA7	38.98	0.219 M $MgCl_2$	13.8	1.13
KA1	39.47	0.219 M $MgCl_2$	12.5	1.17
KA5	37.35	0.657 M NaCl	14.7	1.53
KA41	38.01	DW	14.6	1.48

Creep behavior of KA chalk shows a different trend from that of pure chalks (SK and MO). Cores flooded with 0.657 M NaCl and DW exhibit similarly smaller creep strain (Fig. 11) compared to that of pure chalks (SK and MO). Cores flooded with 0.219 M $MgCl_2$ on the other hand develop an enhanced creep of 2–4 times higher than that flooded with NaCl or DW. The creep rates curves show the pace are doubled compared to that of NaCl or DW. Approximately after 250 h-creep, the extended test (KA1) shows some modest increase in the creep rate. Thereafter for more than 800 h-creep core KA1 demonstrates an enhanced creep strain with a steady growth with time.

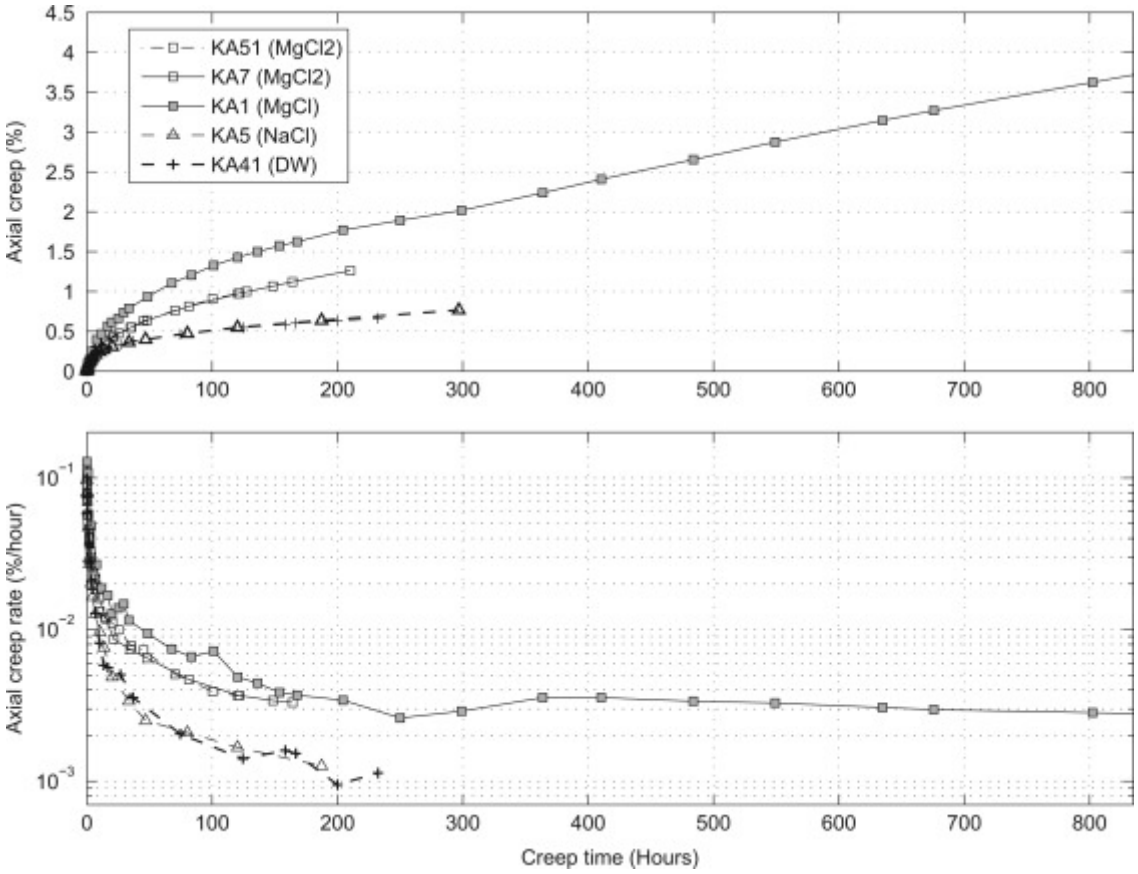

Fig. 11. Axial creep strain (upper) and creep rate (lower) with time of KA cores flooded with 0.657 M NaCl and 0.219 M $MgCl_2$ at 130 °C. Cores flooded with DW and 0.657 M NaCl fall into the same trend. Significant creep enhancement is demonstrated by the cores flooded with 0.219 M $MgCl_2$. The creep also develops with larger rate.

Chemical analyses on the fractioned effluent of core KA7 flooded with 0.219 M $MgCl_2$ and core KA5 flooded with 0.657 M NaCl are shown in Figs. 12 and 13, respectively. Similar behavior as the other chalk types are shown although the amount of Mg^{2+} loss is modest (Fig. 12). Analysis on Silicium content by ICP-OES is also included. The amount of Silicium produced, although low, cannot be disregarded. Such a concentration gives an indication that chemical processes probably do not only involve dissolution on the calcite surfaces but also on the non-carbonate phases. Fig. 12 shows slightly larger Si production for $MgCl_2$ flooding than NaCl (Fig. 13).

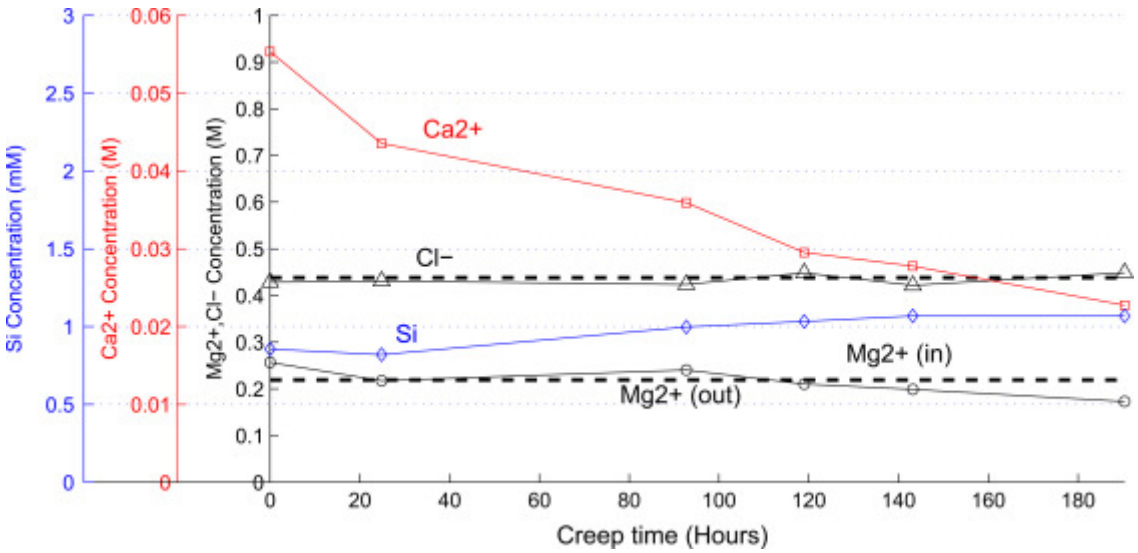

Fig. 12. Mg^{2+}, Ca^{2+}, Cl^{-}, and Si concentrations in the sampled effluents from core KA7, flooded with 0.219 M $MgCl_2$. Original Mg^{2+} and Cl^{-} concentrations are shown by the dashed lines. Note loss of Mg^{2+} and production of Ca^{2+}.

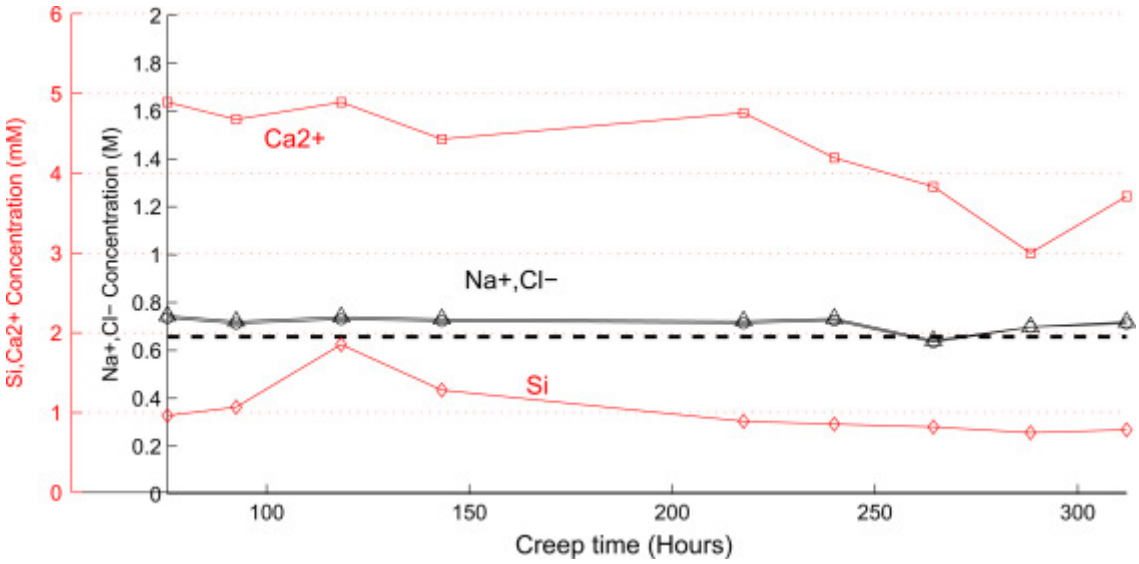

Fig. 13. Na^{+}, Ca^{2+}, Cl^{-}, and Si concentrations in sampled effluents from core KA5, flooded with 0.657 M NaCl. No change in the Na^{+} and only minor production of Ca^{2+}.

3.4. Aalborg

Aalborg chalk is relatively impure with a calcite content of around 95%. Typical characteristics of Aalborg chalk is the abundance of opal-CT, formed in blades and lepispheres, present in the non-carbonate phase.

Stress–strain plot during isotropic loading (Fig. 14) as well as creep plots is highly repeatable when replicating the test with the same fluid. The porosity of the samples are also relatively homogeneous and hence any effect of the different aqueous chemistry is immediately shown. Nevertheless, all the cores flooded with either 0.657 M NaCl or 0.219 M $MgCl_2$ exhibit quite similar behavior in the loading phase. Compared with that of NaCl, the bulk modulus and

yield point of $MgCl_2$-flooded cores may be reduced somewhat (Table 6). The difference is, however, small.

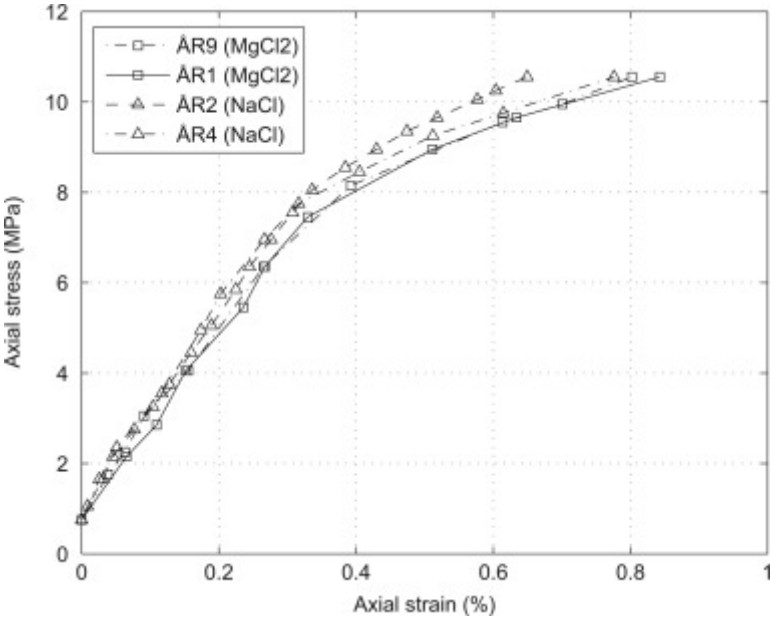

Fig. 14. Axial stress versus axial strain of ÅR cores flooded with 0.657 M NaCl and 0.219 M $MgCl_2$ at 130 °C.

Table 6. Mechanical test results of Aalborg (ÅR) chalk based on isotropic compression in Fig. 14.

Core ID	**Por. (%)**	**Fluid**	**Yield point (MPa)**	**Bulk modulus (GPa)**
ÅR9	46.5	0.219 M $MgCl_2$	8.0	0.70
ÅR1	46.2	0.219 M $MgCl_2$	8.2	0.67
ÅR2	46.2	0.657 M NaCl	8.6	0.75
ÅR4	46.7	0.657 M NaCl	8.1	0.73

Creep behavior of Aalborg chalk is quite similar as that KA chalks. Cores flooded with $MgCl_2$ experience significant dissolution and develop an enhanced creep with a relatively constant rate (Fig. 15). Creep strain for cores exposed to 0.219 M $MgCl_2$ is approximately a factor of 2 larger than those exposed to 0.657 M NaCl. Calcium production under $MgCl_2$ flooding is nearly in the order of magnitude higher than that of NaCl flooding (Figs. 16 and 17). No specific change observed in the pH, which is quite stable in both cases in the range of 8.

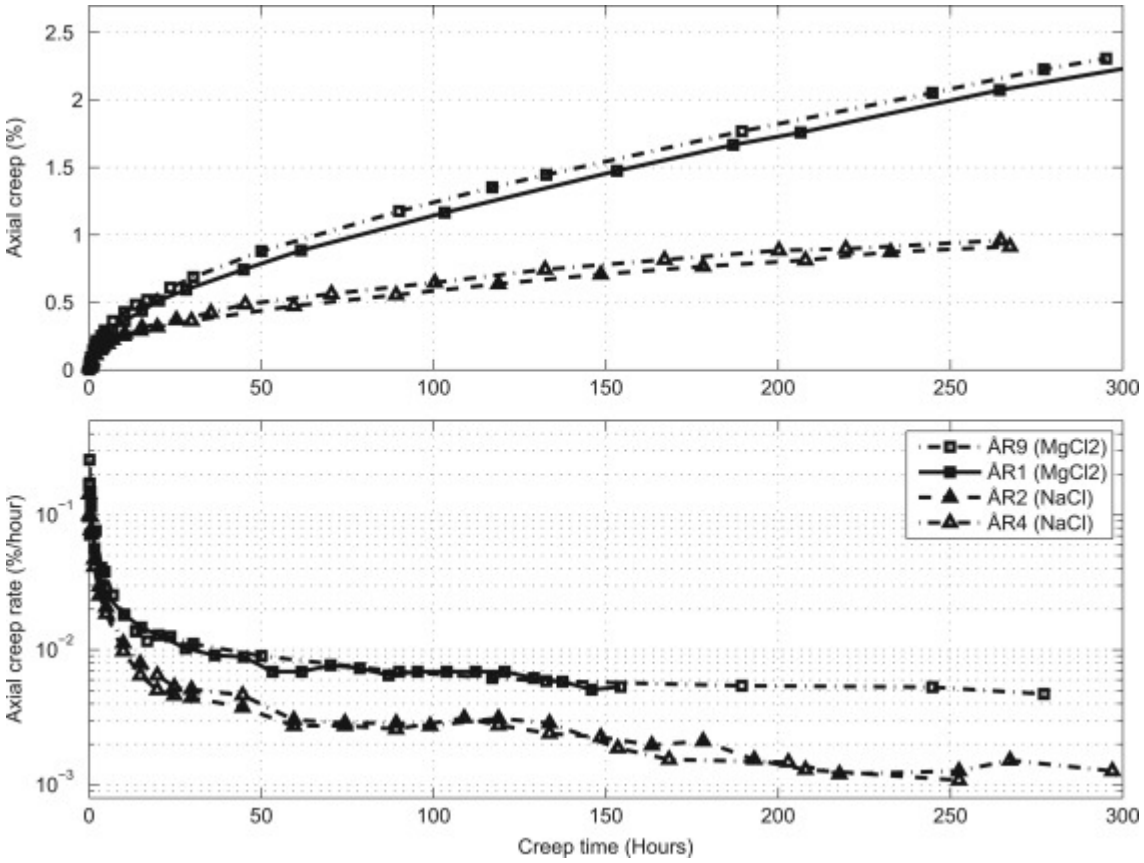

Fig. 15. Axial creep strain (upper figure) and creep rate (lower figure) with time of ÅR cores flooded with 0.657 M NaCl and 0.219 M $MgCl_2$ at 130 °C. Note 2 times larger creep strain developed by the cores exposed to 0.219 M $MgCl_2$ solution, and the creep grows steadily at higher rate with time.

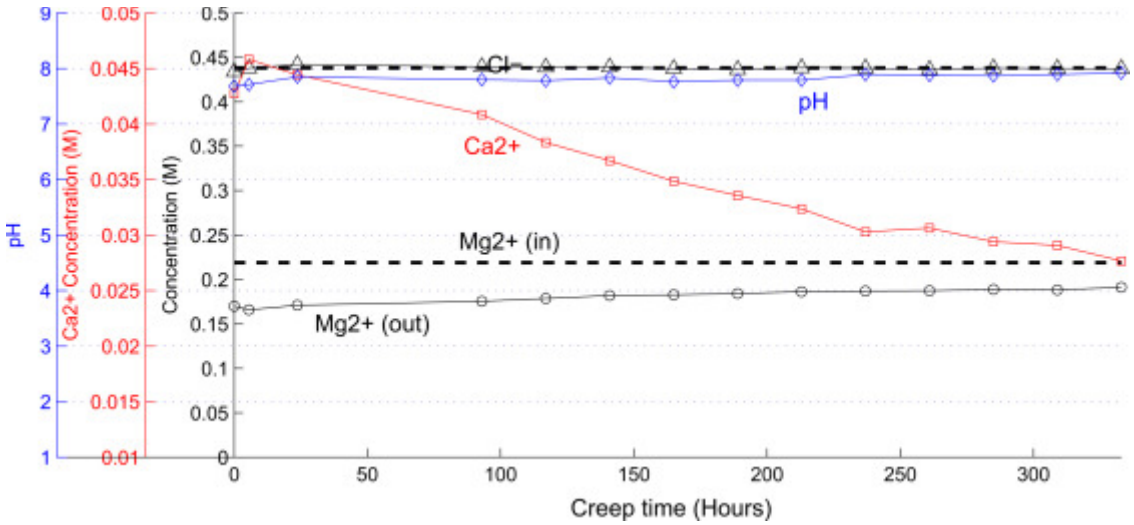

Fig. 16. Mg^{2+}, Ca^{2+}, Cl^- concentrations and pH in sampled effluents from core ÅR1, flooded with 0.219 M $MgCl_2$. Original Mg^{2+} and Cl^- concentrations are shown by dashed line. Note loss of Mg^{2+} and production of Ca^{2+}.

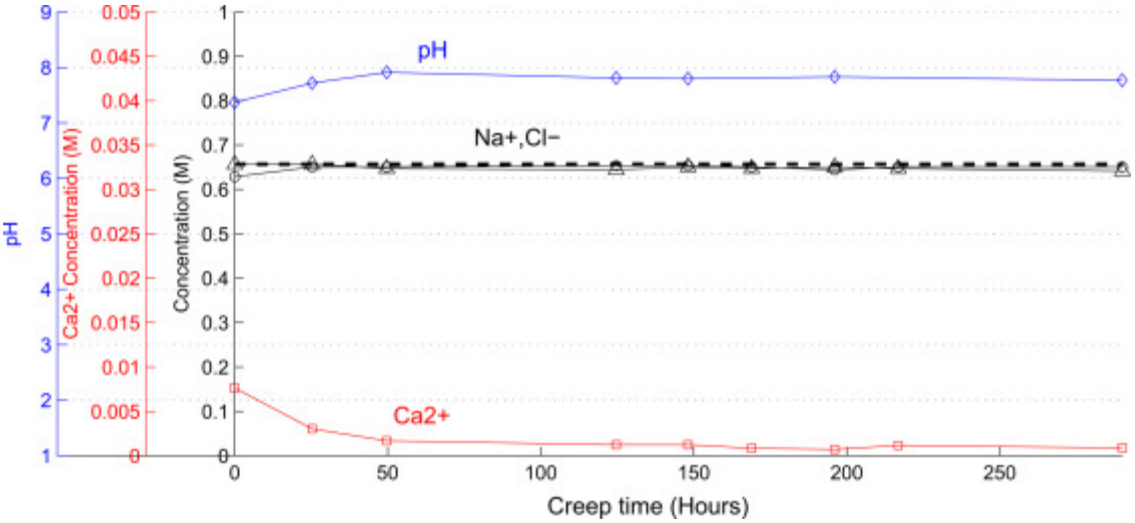

Fig. 17. Na^+, Ca^{2+}, and Cl^- concentrations in sampled effluents from core ÅR2, flooded with 0.657 M NaCl. No change in the Na^+ and only minor production of Ca^{2+}.

Similar to KA chalks, macroscopic creep behavior of ÅR chalk follows the same trend as in the chemical dissolution. Enhancement in the calcite dissolution and the time-dependent creep is demonstrated from the initial creep phase.

3.5. Liége

Liége chalk is also relatively impure with calcite content around 95% similar with Ålborg chalk. Liége chalk commonly exhibits overgrowth and has well-preserved coccoliths (Hjuler, 2007).

Stress versus strain during isotropic loading is shown in Fig. 18. The mechanical properties are also summarized in Table 7. Note that core RL32 is not from the same block, and differences in the bedding direction may result in some difference especially in the loading phase. Nevertheless, core RL32 exposed to NaCl solution and with lower porosity show higher yield and in the plastic phase (after pore collapse), the bulk modulus is stiffer. Samples RL2 and RL11 with comparable porosity however do not seem to show any specific trend according to the specific fluids injected.

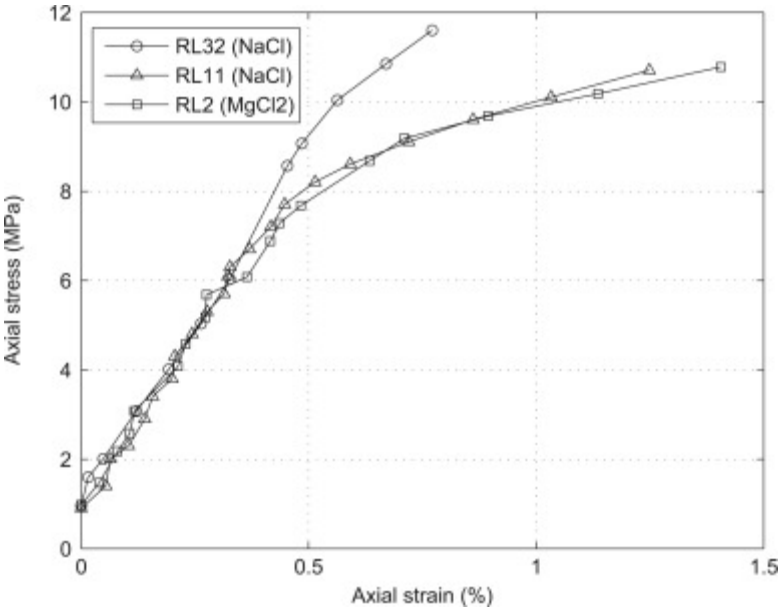

Fig. 18. Axial stress versus axial strain of RL cores flooded with 0.657 M NaCl and 0.219 M $MgCl_2$ at 130 °C.

Table 7. Mechanical test results of Liége (RL) chalk based on isotropic compression in Fig. 18.

Core ID	**Por. (%)**	**Fluid**	**Yield point (MPa)**	**Bulk modulus (GPa)**
RL2	41.1	0.219 M $MgCl_2$	7.6	0.49
RL11	41.2	0.657 M NaCl	7.6	0.55
RL32	40.1	0.657 M NaCl	9.5	0.59

Creep deformation and rates in RL chalk show similar behavior as the other impure chalks (KA and ÅR) (Fig. 19). The difference between core RL11 and RL32, both flooded with 0.657 M NaCl, is apparently related to the porosity. Between the different aqueous chemistry, core RL2 flooded with 0.219 $MgCl_2$ clearly demonstrates an enhanced creep deformation with a factor 2 higher than that flooded with 0.657 M NaCl. The creep also develops with three times faster pace than that of 0.657 M NaCl.

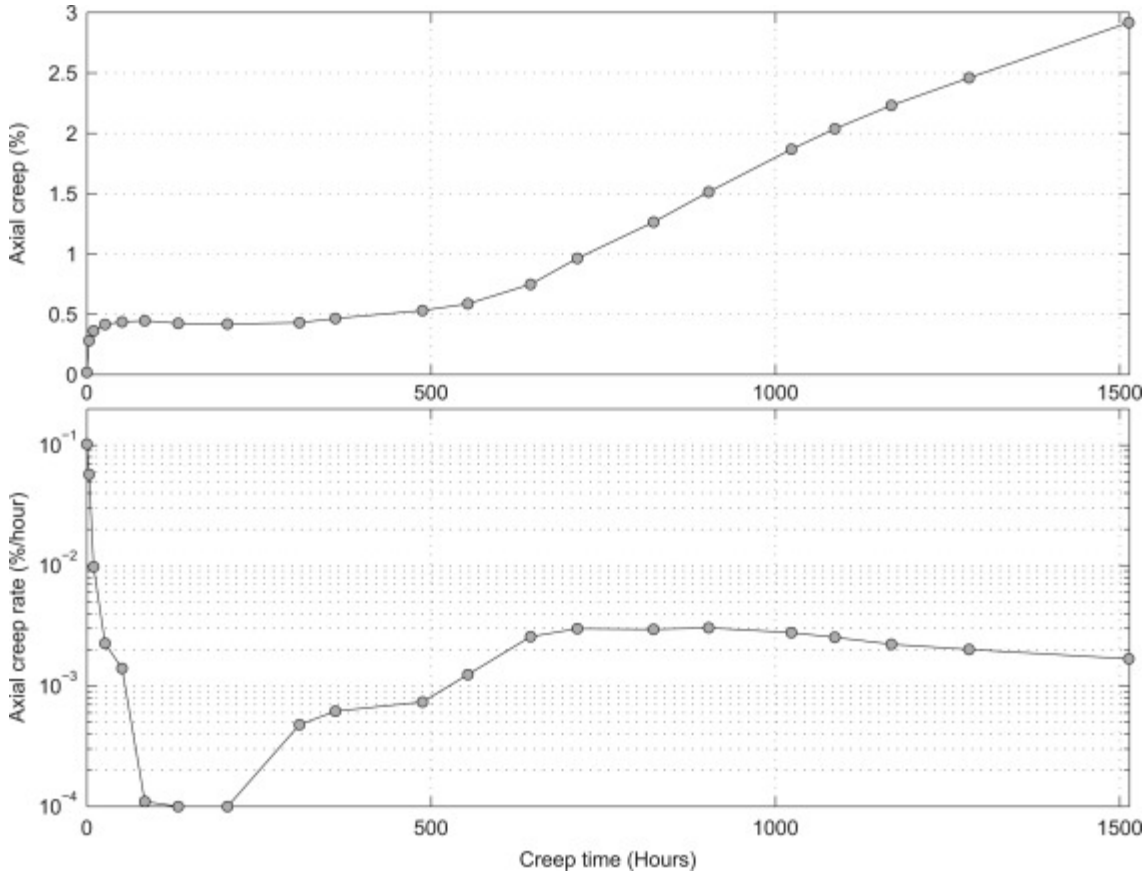

Fig. 19. Axial creep strain (upper) and creep rate (lower) with time of RL cores flooded with 0.657 M NaCl and 0.219 M $MgCl_2$ at 130 °C. Note 2–4 times larger creep strain for RL2 core exposed to 0.219 M $MgCl_2$ solution. The creep also develops with approximately a magnitude higher.

Chemical analysis as presented in Madland et al. (2011) show that RL chalk exposed to 0.219 M $MgCl_2$ solution experiences constant loss of Mg^{2+} and in the same time constant production of Ca^{2+} is demonstrated. For cores flooded with 0.657 M NaCl, however, negligible net chemical change is demonstrated. In summary, similar to those KA and ÅR chalks, enhanced dissolution and enhanced time-dependent creep for RL chalk follow the same trend and they occur from the primary creep phase.

4. Discussion

4.1. Implication in the porosity–permeability relationship

From the differential pressure across the core plug and with known flooding rate, final permeability at the end of the creep test was calculated according to Darcy's equation. Kozeny's equation has been used to describe the relation between porosity–permeability as follows:

(3) $$\kappa = c\,\frac{\phi^3}{S^2} = c\,\frac{(\phi)^3}{(1-\phi)^2 \cdot S_g^2}$$

In Mortensen et al. (1998), parameter c is formulated as a function of porosity as follows:

(4) $$c(\phi) = [4\cos(\tfrac{1}{3}\arccos(\phi \cdot 2 - 1) + \tfrac{4}{3}\pi) + 4]^{-1}$$

where S is the grain surface area per bulk volume, and S_g is grain-surface area per grain volume as measured by BET specific surface area.

Final porosity (ϕ) when the core plug has experienced some axial deformation (ϵ_a) is calculated as follows:

$$\phi = \frac{\phi_0 - 3 \cdot \epsilon_a}{(1 - 3 \cdot \epsilon_a)} \quad (5)$$

where ϕ_0 is the initial porosity. We have assumed that the change of solids volume is negligible and that volumetric strain under isotropic compression will decrease the pore volume.

The relationship between initial porosity and liquid permeability before isotropic loading (0.5 MPa confining pressure), and the relationship between final porosity and permeability (at respective creep stress levels) at the end of the test are illustrated in Figs. 20 and 21, respectively.

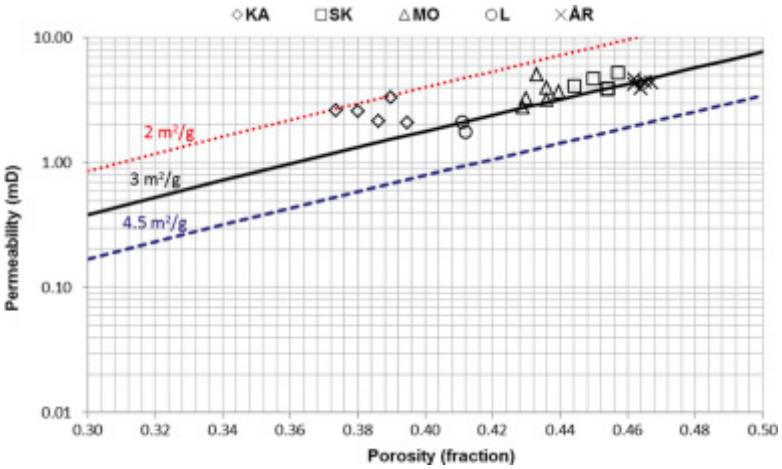

Fig. 20. Initial correlation of porosity vs. permeability before the creep test. Lines are Kozeny correlation (Eq. (3)) for constant specific surface area (SSA). Note Kozeny-derived SSA are in good agreement with measured SSA by BET (N_2) listed in Table 1.

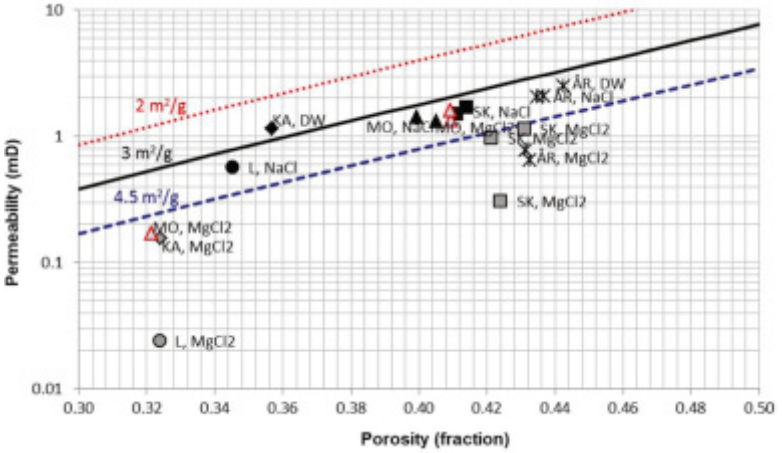

Fig. 21. Final correlation of porosity vs. permeability at the end of creep test. Lines are Kozeny correlation (Eq. (3)) for constant specific surface area (SSA). Note clear split between NaCl-exposed and $MgCl_2$-exposed cores. All the NaCl data stay within the initial SSA, while those of $MgCl_2$ have been shifted towards larger SSA (outside the two bounds).

From the initial porosity vs. permeability, all the data points are generally grouped within the same lines, corresponding to a specific surface area of 3–4 m^2/g (Fig. 20). This value is quite consistent with BET(N_2) measurement as mentioned in the materials section above (Table 1).

In the final porosity vs. permeability, data points from NaCl and $MgCl_2$ flooding show a clear split (Fig. 21). Those of NaCl or DW flooding stay within the same SSA line. In this case the change of porosity vs. permeability relationship is only caused by the volumetric strain experienced by the cores. No alteration on the chalk surface is indicated as the data points are generally shifted within the same SSA line. For the cores exposed to $MgCl_2$, however, the porosity–permeability relationships have been shifted to different specific surface area lines. The specific surface area for the majority of the data points is increased to more than 5 m^2/g. For Liége the increase is dramatic, approximately 15 m^2/g. Such marked change indicates significant alteration on the chalk surface, apparently induced by the chemical processes in accordance with the behavior observed in the aqueous chemistry analysis.

Summing up, significant chemical alterations on the chalk surface are obviously indicated by a significant increase in the specific surface area for cores exposed to 0.219 M $MgCl_2$ solution.

4.2. Implication in the chalk microstructure

Microscopic analysis by SEM (Scanning Electron Microscopy) has been performed on Kansas and Liége chalks. In Fig. 22 SEM image on tested core KA1 sample subjected to a prolonged creep with continuous $MgCl_2$ injection is shown. Chemical alterations are shown by the presence of newly precipitated minerals which appear as granules or sometimes fused as aggregates locally filling the pore space (Fig. 22(a)). A-well defined cube crystal indicated as magnesite is also identified (Fig. 22(b)).

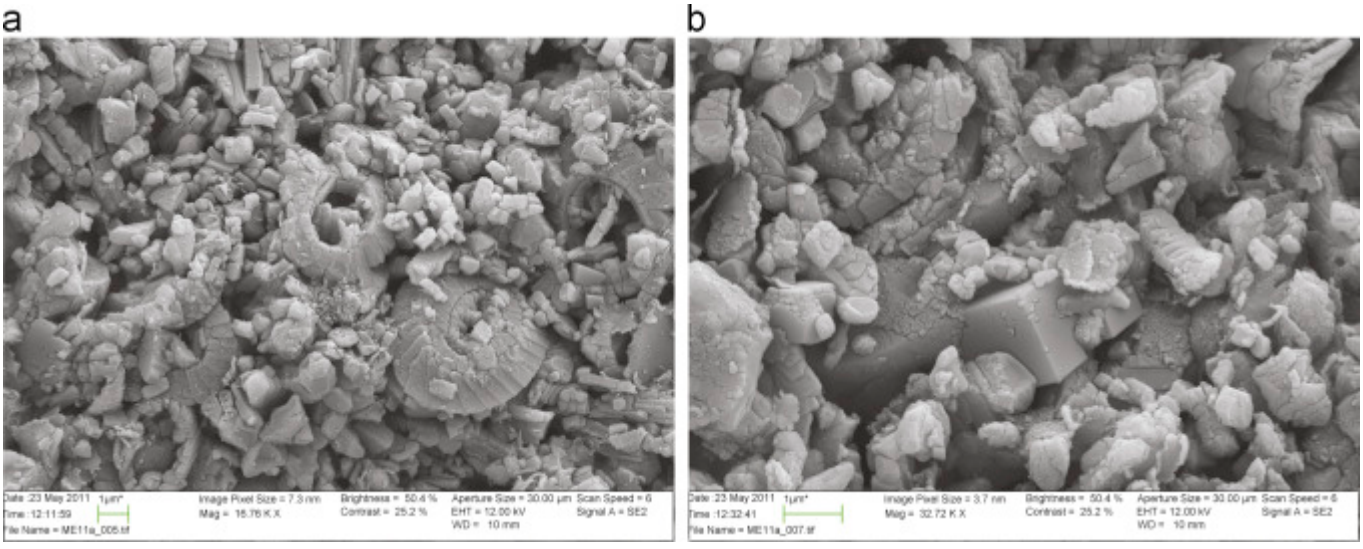

Fig. 22. SEM analysis of KA1 flooded with 0.219 M $MgCl_2$ after creep test is ended. Images are taken at regions close to the inlet area. Left figure shows evidence of newly precipitated minerals which appears as granular or aggregates. Right figure shows a zoomed-in image showing a crystal cube precipitate, which according to EDS analysis, may be interpreted as magnesite.

Microscopic study by X-ray diffraction and BET (N_2) specific surface area analyses on Liége chalk subjected to long term creep test with continuous injection of $MgCl_2$ solution of more than 1 year is summarized in Fig. 23. A complete change in the textural properties from the

core inlet to outlet is shown. BET (N_2) analysis on the sliced parts shows that the specific surface area has been doubled. These BET(N_2) analyses strongly support the increase of specific surface area derived from the porosity–permeability relationships (Fig. 21). XRD analysis on the core inlet slice shows strong indication of the presence of Magnesite. Quantitative analysis on the XRD spectrum shows that more than 50% of the tested chalk materials have been transformed into Magnesite, formed particularly near the core inlet.

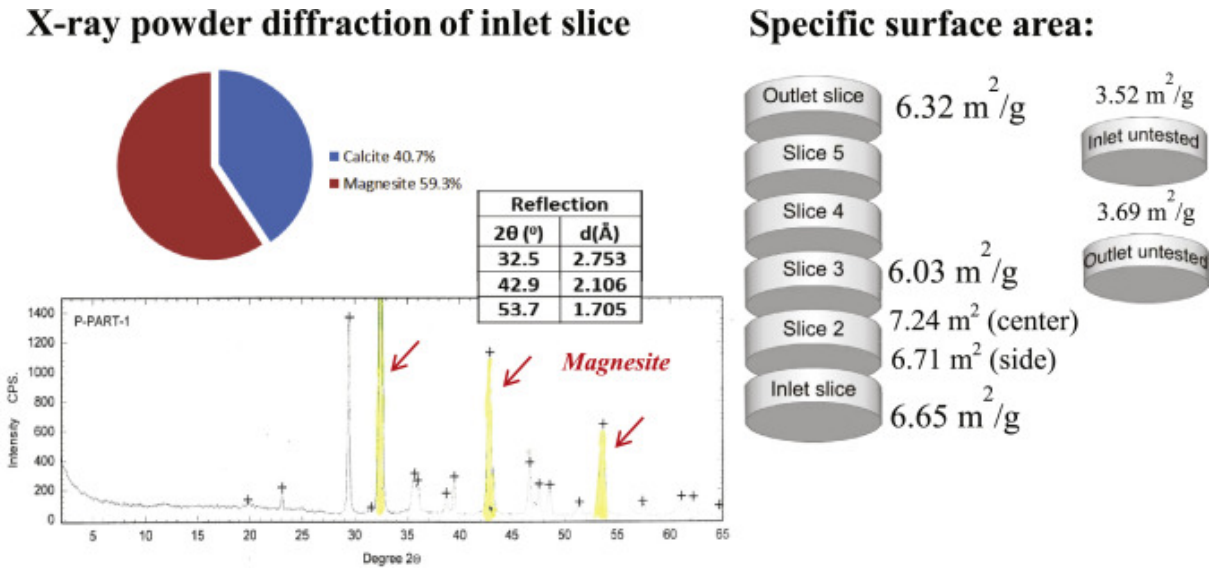

Fig. 23. Evidence of chemical alteration as shown by increased specific surface area from BET analysis and changes in mineralogy from XRD. Liége core after long-term creep test with continuous injection of 0.219 M $MgCl_2$ at 130 °C.

Continuous loss of Mg^{2+} has been shown by all the chalk cores flooded with 0.219 M $MgCl_2$ brine. Clearly such retention of Mg^{2+} is present in the newly precipitated minerals and not on the calcite grains. Chemical alterations have also involved the non-carbonate phase as shown by the chemical analyses where Si is detected in the effluent (see Fig. 12).

4.3. Implication in the creep deformation

Cumulative calcite dissolution at time *t* has been calculated as follows:

(6) Ca produced (mmol) $= Q \int_{t0}^{t} m_{Ca2+}\, dt,$

where m_{Ca2+} is the calcium concentration in the effluent solution (mol/L), *Q* is the injection rate (mL/s), and *t* is the length of time since introduction of the respective brine.

All results from the 5 chalk types show that injection of $MgCl_2$ has caused significant dissolution, where the concentration of Ca^{2+} produced is well-maintained with continuous supply of fresh fluid. The excess of Ca^{2+} production during $MgCl_2$ flooding can then be calculated from the extra calcium produced relative to that of NaCl flooding. Cumulative calcium production of $MgCl_2$ and NaCl flooding generally exhibit a linear relationship with time, as shown in Fig. 24 and Table 8.

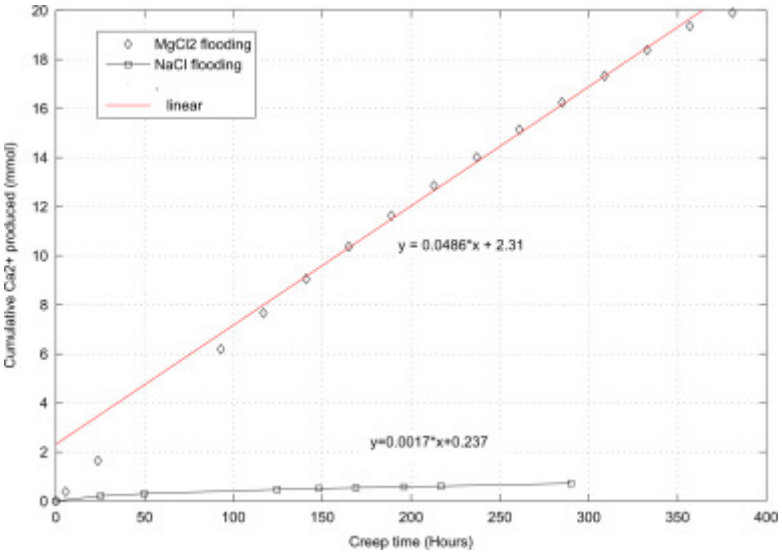

Fig. 24. Illustration of Cumulative Ca^{2+} in the core effluent with time. Samples shown are ÅR1 and ÅR2 flooded with 0.219 M $MgCl^2$, and 0.657 M NaCl, respectively

Table 8. Linear correlation of cumulative Ca^{2+} with time obtained from effluent analysis by IC Chromatograph. *y* is the cumulative Ca^{2+} in mmol, *t* is the creep time in hours.

Chalk type	**0.657 M NaCl (mmol)**	**0.219 M $MgCl_2$ (mmol)**
Aalborg	$y = 4.86 \cdot 10^{-2} \cdot t + 2.31$	$y = 1.70 \cdot 10^{-3} \cdot t + 0.237$
Kansas	$y = 2.97 \cdot 10^{-2} \cdot t + 2.70$	$y = 5.70 \cdot 10^{-3} \cdot t + 0.03$
Liége	$y = 4.12 \cdot 10^{-2} \cdot t + 2.91$	$y = 6 \cdot 10^{-3} \cdot t + 0.451$
Mons	$y = 3.43 \cdot 10^{-2} \cdot t - 7.37$	$y = 0.6 \cdot 10^{-3} \cdot t + 0.02$
Stevns Klint	$y = 3.31 \cdot 10^{-2} \cdot t + 1.04$	$y = 2.3 \cdot 10^{-3} \cdot t - 0.007$

All the pure chalks (SK and MO) have consistently shown that creep enhancement does not occur from initial time, but rather a delayed response. The onset of creep enhancement, as shown by a tertiary-like phase, is characterized by a distinct acceleration in the Ca^{2+} production and simultaneously an acceleration in the creep pace. The creep excess in such a case can be therefore calculated from the difference between the measured creep relative to the rate-type model as follows:

(7) $\text{Excess Creep} = \text{Measured Creep} - (A \ln(1 + t/t_0))\text{MgCl}_2$

Fig. 25 shows that before the tertiary-like creep evolves, the creep behavior is sufficiently captured by the rate-type model. The difference between the two curves (measured creep and the extrapolated model) would therefore give some quantification on the contribution from the chemical effects.

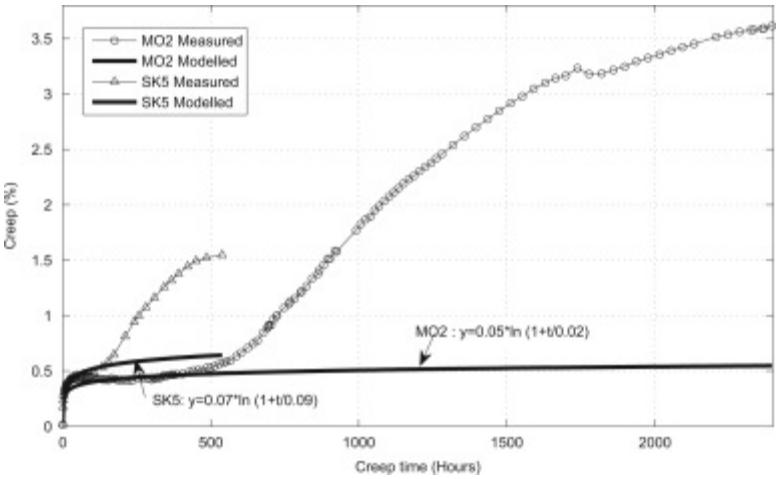

Fig. 25. Measured and modelled creep for $MgCl_2$ -flooded cores according to the rate-type model Eq. (1). The primary phase before the acceleration is sufficiently captured by the model.

For the impure chalks (RL, KA, and ÅR) exposed to $MgCl_2$ solution, as presented above, the creep deformation is enhanced from the initial time. Unlike that of pure chalks, the chemical effect alone cannot be immediately distinguished. Here the contribution from chemical effects is therefore taken from the creep difference between $MgCl_2$ and NaCl flooding. Since the duration of creep test between $MgCl_2$ and NaCl is different, the rate-type model fitted to the measured creep from NaCl-flooded core is instead used. This approach is supported by the excellent agreement between the rate-type model and the measured creep from all the impure chalk cores exposed to NaCl (Fig. 26). Such agreement confirms that in the absence of chemical effect, creep behavior can be sufficiently described by the rate-type model. The excess of creep strain for impure chalks is therefore calculated relative to that of NaCl flooding as follows:

(8) Excess Creep = Measured Creep − $(A \ln(1 + t/t_0))$NaCl

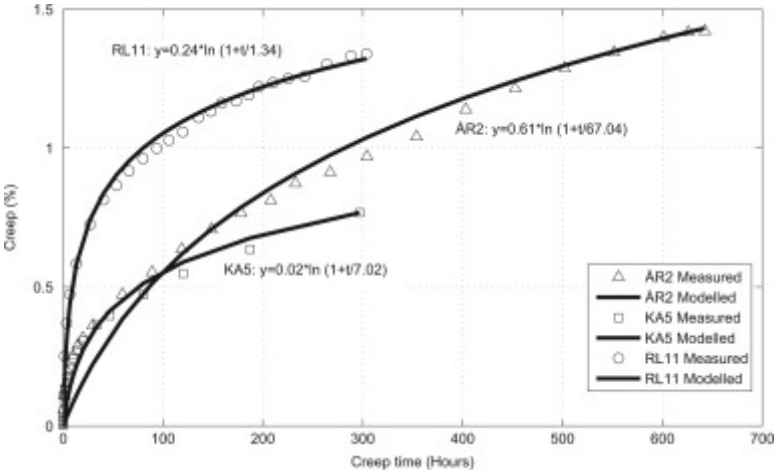

Fig. 26. Measured and modelled creep for NaCl-flooded cores according to the rate-type model Eq. (1). Note for NaCl-flooding, good match with the data is demonstrated.

Relationships between excess dissolution and the additional creep are shown in Fig. 27. A systematic correlation for all the chalk types tested is consistently demonstrated. The later stage where creep steadily develops is taken for the best fit (Table 9). The results show that

when a minimum calcite dissolution is overcome, the chemically induced creep with time can be well-correlated with the amount of dissolution (Table 9).

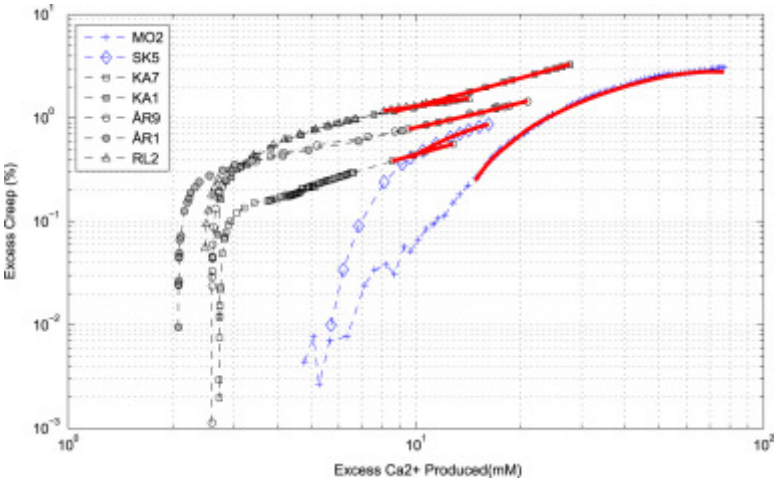

Fig. 27. Systematic correlation between calcite dissolution and the creep strain measured from all the chalk cores flooded with 0.219 M $MgCl_2$. The steady-state part marked with red line are taken for best fit as shown in Table 9.

Table 9. Correlation between excess calcium and the resulting excess creep from the best fit in Fig. 27. $\Delta\epsilon$ is excess creep (%), Δm_{Ca} is the excess Ca^{2+} produced (mmol).

Chalk type	**Excess creep (%)**
Aalborg	$\Delta\epsilon = 0.06 \cdot \Delta m_{Ca} + 0.21$
Kansas (KA7)	$\Delta\epsilon = 0.04 \cdot \Delta m_{Ca} + 0.02$
Kansas (KA1)	$\Delta\epsilon = 0.11 \cdot \Delta m_{Ca} + 0.17$
Liége	$\Delta\epsilon = 0.06 \cdot \Delta m_{Ca} + 0.68$
Mons	$\Delta\epsilon = -0.8 \cdot 10^{-3} \cdot \Delta m^2_{Ca} + 0.12 \cdot \Delta m_{Ca} - 1.43$
Stevns Klint	$\Delta\epsilon = -3.4 \cdot 10^{-3} \cdot \Delta m^2_{Ca} + 0.16 \cdot \Delta m_{Ca} - 0.80$

It can be seen that creep enhancement for all the impure chalks (KA, ÅR, and RL) evolve immediately, after about 2–3 mmol cumulative Ca^{2+} produced. In addition, the effect of dissolution on the time-dependent creep at steady state can be sufficiently described by a linear correlation. For the pure chalks (SK and MO), however, creep enhancement is more gradual. It requires higher calcite to dissolve (5 mmol cumulative Ca produced) before any creep acceleration evolves. When the excess Ca^{2+} production is higher than 10 mmol, the best-fit rather exhibits a second order correlation. Clearly all the results show a systematic correlation between excess dissolution and the corresponding creep (Fig. 27 and Table 9). The exactness of the correlation is not important here, but the best fits clearly demonstrate direct correlation on how dissolution controls the deformation behavior of chalk over time.

The time-dependent response between pure and impure chalk is interesting. Creep in chalk has been commonly described as a cascade of failure redistribution process. The main mechanism underlying the rate-type creep model is the off-sliding asperities under friction between granular contacts (Andersen et al., 1992; Andersen, 1995). High-porosity chalks are commonly characterized as coccolith fragments stacked together in irregular structure with poor cementation, resulting in a weak structure.

Calcite dissolution can change the morphology of calcite surfaces in terms of grain rounding and negative crystal formation having prism and/or rhombohedral faceted faces (Gautier et al., 2001). Grain rounding may decrease the intergranular friction, and thus favoring the creep mechanisms.

Precipitation triggers enhanced dissolution but on the other hand it may also increase the intergranular friction and hence increased resistance against the creep deformation. Such mechanisms may explain the negative terms in the quadratic correlation of dissolution-creep deformation from the pure chalks (Table 9).

In impure chalks, where creep enhancement occurs immediately, chemical alterations have apparently involved the non-carbonate phase, eventually providing an additional effect which overcomes the frictional behavior. Chemical alterations on the non-carbonate phases in the present study are addressed from dissolution–precipitation, although it is clearly not limited to these effects only. The non-carbonate phase commonly fills the intergranular voids, and acts as contact cement holding the calcite grains together (Fabricius et al., 2007). It is possible that dissolution of the non-carbonate phases can be a precursor to slide off the support carried by the granular contact points and thus furthering the deformation. The presence of clay minerals, which furthers diffuse transport along grain boundaries (Renard et al., 2001), will have also important consequences on the dissolution–precipitation. The detailed chemical processes in the non-carbonate minerals are beyond the scope of this paper.

For pure chalks (Stevns Klint and Mons), there is negligible contribution from the non-carbonate dissolution. The creep initially diminishes before it starts to accelerate. In favor to the rate-type creep model, the delay of creep enhancement in MO and SK chalks may be associated with the time required for calcite dissolution to overcome the intergranular friction.

Creep acceleration which appears as a tertiary creep coincides with an increase in the Ca^{2+} production, where the concentration is well-maintained. The calcite dissolution rate has increased from 0.72 (lowest point) to 0.84 mmol/day for SK5 (Fig. 3) and from 0.35 (lowest point) to 0.83 mmol/day for MO2 (Fig. 8). No major change in the concentration of Mg^{2+} is however shown. Because dissolution changes the morphology of calcite surfaces progressively, the increase in the dissolution rate must be surface-related mechanisms. AFM studies (Shiraki et al., 2000; Xu et al., 2010) show that dissolution of calcite {104} surfaces occurs through rhombohedral pitch development where the crystallographic orientations determine the dissolution rate (Smith et al., 2013). These indicate that progression of calcite surface morphology through alteration of significant part of chalk volume is required before an increase in the dissolution rate starts. When the onset of creep acceleration occurs, this may also escalate the failures process, generating new surface areas of highly kinked morphology subject to greater Ca^{2+} release (Hu and Hueckel, 2007; Smith et al., 2013). The deformation and dissolution therefore can be a coupled process.

Hellmann et al. (2002b) argue that dispersion does occur within chalk where some fluid bypasses the matrix whereas others percolate much more slowly over longer time scale than the fluid residence. Averaged ionic diffusion in free water at 130 °C according to Appelo and Postma (2005) can be calculated as follows:

(9) $$D_{f,T} = \frac{D_{f,298} \cdot T \cdot \eta_{298}}{298 \cdot \eta_T}$$

where η is the water viscosity and T is the temperature (K). An average diffusion ionic diffusion ($D_{f,298}$) of $7.4 \cdot 10^{-9} m^2/s$ at 25 °C will correspond to $7.4 \cdot 10^{-9} m^2/s$ at 130 °C. In 0.07 m long core plug this will mean a 183 h-diffusion time. It should be mentioned that the exact diffusion coefficient in porous media requires a more rigorous calculation which includes several parameters such as tortuosity, electrical resistance property, and a statistical approach. The diffusion time calculated from the free-water diffusion above, nevertheless, gives a time scale which is in good agreement with the creep acceleration onset in SK5 (150 h) and MO2 (300 h) chalks. In this respect if most of the fluid flow infiltrates the channels (Hellmann et al., 2002b), the time lag demonstrated in the pure chalks should therefore correspond to the diffusion time. This would imply that calcite dissolution involves not only the free-face but also the intergranular micropores area, which in turn affect the intergranular friction.
Comparison between the time-dependent creep response from the impure and pure chalks has clearly shown that the presence of non-carbonate minerals has a major influence on the onset of chemically induced mechanical degradation. Systematic correlation and microscopic analyses have provided a link between dissolution–precipitation and the time-dependent deformation in high-porosity chalks.

5. Conclusion

Extensive rock mechanical tests on Kansas, Liége, Aalborg, Stevns Klint, and Mons chalks were performed under isotropic stress above the yield point and with continuous injection of NaCl and $MgCl_2$ solutions at 130 °C. Chemical alterations on chalk cores flooded with $MgCl_2$ solutions are demonstrated by significant change in the aqueous chemistry, change in the microstructures by SEM-EDS, XRD, and BET (N_2) analyses and most importantly by change in the porosity–permeability relationship. No such changes are demonstrated by cores flooded with 0.657 M NaCl solutions. The chemical effects have been described as precipitation–dissolution which impacts the time-dependent deformation behavior.

Systematic correlation between calcite dissolution and the additional creep strain is demonstrated by all the different chalk types. Steady state creep behavior for all the impure chalks can be sufficiently described by a linear correlation with the calcium produced. For pure chalks the steady state creep show a squared-dependency with the calcite dissolution.

Chemical alterations have signified the role of non-carbonate dissolution as well as carbonate dissolution and the precipitation of new secondary minerals. Creep deformation in pure chalks such as Stevns Klint and Mons are characterized by an initial stage of creep diminution before a-tertiary-like creep subsequently evolves with an accelerated rate. Diminution of creep is described as the time for dissolution to overcome intergranular friction. Creep acceleration and enhanced calcite dissolution are aligned in time. Enhanced dissolution has been explained by progression of calcite surface morphology to alter significant chalk volume and/or slow fluid diffusion to reach micropores areas.

For impure chalks (Liége, Kansas, and Aalborg) the impact of dissolution is demonstrated immediately after 2–3 mmol cumulative calcium produced. The combined effects of chemical alterations on the non-carbonate and carbonate phases outweigh the effect intergranular friction and hence resulting in an immediate creep enhancement, which develops from the primary creep phase.

Acknowledgment
The authors thank University of Stavanger for the financial support of the present study. We also thank the industry partners of the National IOR Centre of Norway including ConocoPhillips Skandinavia AS, BP Norge AS, Det Norske Oljeselskap AS, Eni Norge AS, Maersk Oil Norway AS, DONG Energy A/S Denmark, Statoil Petroleum AS, GDF SUEZ E&P NORGE AS, Lundin Norway AS, Halliburton AS, Schlumberger Norge AS, Wintershall Norge AS. Cameron Strachan is acknowledged for checking the language. Prof. Lawrence M. Cathles from Cornell University is acknowledged for the valuable discussions.

References

Andersen, M. (1995) Petroleum Research in North Sea Chalk. RF Rogaland Research, Stavanger, Norway

Andersen, M.A., Foged, N., Pedersen, H.F., (1992) The rate-type compaction of a weak North Sea chalk. In: Proceedings of the 33rd U.S. Symposium (eds J.R. Tillerson and W.R.W. Wawersik), A.A. Balkema, Rotterdam, 253-261.

Appelo, C., D. Postma, D. (2005) Geochemistry, Groundwater and Pollution. (2nd edition), Taylor and Francis Group, Leiden, The Netherlands

Baker, P.A., Kastner, M. J., Byerlee, D., Lockner, D.A. (1980) Pressure dissolution and hydrothermal recrystallization of carbonate sediments-an experimental study**.** Mar. Geol., 38, pp. 185-203

Bjørkum, P., Nadeau, P. (1998) Temperature controlled porosity/permeability reduction, fluid migration, and petroleum exploration in sedimentary basins**.** Aust. Pet. Prod. Explor. Assoc. J., 38, pp. 453-464

Durney, D. (1972) Solution transfer—an important geological deformation mechanism. Nature, 235, pp. 315-317

Ehrenberg, S., Eberli, G., Keramati, M., Moallemi, S. (2006) Porosity–permeability relationships in interlayered limestone-dolostone reservoirs. AAPG Bull., 90, pp. 91-114

Fabricius, I., Høier, C., Japsen, P., Korsbech, U. (2007) Modelling elastic properties of impure chalk from South Arne Field, North Sea. Geophys. Prospect., 55, pp. 487-506

Fabricius, I.L., Borre, M. (2007) Stylolites, porosity, depositional texture, and silicates in chalk facies sediments. Ontong java plateau-Gorm and Tyra fields, North Sea. Sedimentology, 54, pp. 183-205

Garrison, R.E., Kennedy, W.J. (1977) Origin of solution seams and flaser structure in upper cretaceous chalks of Southern England. Sediment. Geol., 19, pp. 107-137

Gautier, J., Oelkers, E., Schott, J. (2001) Are quartz dissolution rates proportional to bet surface areas? Geochim. Cosmochim. Acta, 65, pp. 1059-1070

Heggheim, T., Madland, M.V., Risnes, R., Austad, T. (2005) A chemical induced enhanced weakening of chalk by seawater**.** J. Pet. Sci. Eng., 46, pp. 171-184

Hellmann, R., Gaviglio, P., Renders, P.N., Gratier, J.P., Bekri, S., Adler, P. (2002a) Experimental pressure solution compaction of chalk in aqueous solutions. Part 2. Deformation examined by SEM, porosimetry, synthetic permeability, and X-ray computerized tomography**.** R. Hellmann, S.A. Wood (Eds.), Water–Rock Interactions, Ore Deposits, and Environmental Geochemistry: A tribute to David A. Crerar. Geochemical Society, pp. 153-178

Hellmann, R., ARenSders, P.N., Gratier, J.P., Guiguet, R. (2002b) Experimental pressure solution compaction of chalk in aqueous solutions. Part 1. Deformation behavior and chemistry**.** R. Hellmann, S.A. Wood (Eds.), Water–Rock Interactions, Ore Deposits, and Environmental Geochemistry: A tribute to David A. Crerar. Geochemical Society, pp. 129-152

Hjuler, M.L., (2007). Diagenesis of Upper Cretaceous Onshore and Offshore Chalk from the North Sea Area (Ph.D. thesis). Institute of Environment & Resources. Technical University of Denmark, Kgs., Lyngby. (Http://www.er.dtu.dk/publications/fulltext/2007/MR2007-134.pdf.)

Hjuler, M.L., Fabricius, I.L., (2009) **E**ngineering properties of chalk related to diagenetic variations of upper cretaceous onshore and offshore chalk in the North Sea area**.** J. Pet. Sci. Eng., 68, pp. 151-170

Hu, L.B., Hueckel, T. (2007) Creep of saturated materials as a chemically enhanced rate-dependent damage process. Int. J. Numer. Anal. Methods Geomech., 31, pp. 1537-1565

Hueckel, T., Hu, L.B. (2007) Coupled chemo-mechanics of intergranular contact: toward a three-scale model. Comput. Geotech., 34, pp. 306-327

Korsnes, R.I., Madland, M.V., Austad, T., (2006a). Impact of brine composition on the mechanical strength of chalk at high temperature. In: Eurock 2006 Multiphysics Coupling and Long Term Behaviour in Rock Mechanics. Taylor and Francis Ltd, London.

Korsnes, R.I., Strand, S., Hoff, O., Pedersen, T., Madland, M.V., Austad, T., (2006b). Does the chemical interaction between seawater and chalk affect the mechanical properties of chalk? In: Eurock 2006 Multiphysics Coupling and Long Term Behaviour in Rock Mechanics. Taylor and Francis Ltd, London

Korsnes, R.I., Madland, M.V., Austad, T., Haver, S., Rosland, G. (2008) The effects of temperature on the water weakening of chalk by seawater**.** J. Pet. Sci. Eng., 60, pp. 183-193

Laronne Ben-Itzhak, L., Aharonov, E., Toussaint, R., Sagy, A., (2012) Upper bound on stylolite roughness as indicator for amount of dissolution. Earth Planet. Sci. Lett., 337-338, 386-396. • DOI: 10.1016/j.epsl.2012.05.026.

Lydzba, D., Pietruszczak, S., Shao, J.F. (2007) Intergranular pressure solution in chalk: a multiscale approach. Comput. Geotech., 34, pp. 291-305

Madland, M.V., Hiorth, A., Omdal, E., Megawati, M., Hildebrand-Habel, T., Korsnes, R.I., Evje, S., Cathles, L.M. (2011) Chemical alterations induced by rock–fluid interactions when injecting brines in high porosity chalks. Transp. Porous Media, 87, pp. 679-702

Megawati, M., Andersen, P., Korsnes, R., Hiorth, H., Madland, M., (2011). The effect of aqueous chemistry ph on the time-dependent deformation behaviour of chalk experimental and modelling study. In: Pore2Fluid IFP Energies Nouvelles, Paris, France, November 16–18.

Mortensen, J., Engstrøm, F., Lind, I. (1998) The relation among porosity, permeability, and specific surface of chalk from the Gorm field, Danish North Sea. SPE Reserv. Eval. Eng., 1, pp. 245-251

Newman, G. (1983) The effect of water chemistry on the laboratory compression and permeability characteristics of some north sea chalks**.** J. Pet. Technol., 35, pp. 976-980

Nguyen, S.H., (2008). Determination of Carbonates by Titration. Retrieved from Sediment Laboratory, Danish Technical University, Lyngby.

Piau, J., Maury, V. (1994) Mechanical Effects of Water Injection on Chalk Reservoirs. Eurock, A.A. Balkema, Delft

Pietruszczak, S., Lydzba, D., Shao, J.F. (2006) Modelling of deformation response and chemo-mechanical coupling in chalk. Int. J. Numer. Anal. Methods Geomech., 30, pp. 997-1018

Renard, F., Dysthe, D., Feder, J., Bjørlykke, K., Jamtveit, B. (2001) Enhanced pressure solution creep rates induced by clay particles: experimental evidence in salt aggregates. Geophys. Res. Lett., 28 (2001), pp. 1295-1298

Renard, F., Schmittbuhl, J. Gratier, J., Meakin, P., Merino, E. (2004) Three-dimensional roughness of stylolites in limestone**.** J. Geophys. Res., 109, p. B03209

Rhett, D.W., Teufel, D.W. (1991) Water-induced shear fracturing in the ekofisk field. Roegiers (Ed.), Rock Mechanics as a Multidisciplinary Science, Balkema, Rotterdam (1991)

Risnes, R., Flaageng, O. (1999) Mechanical properties of chalk with emphasis on chalk–fluid interactions and micromechanical aspects. Oil & Gas Sci. Technol.—Rev. IFP, 54 (6), pp. 751-758

Risnes, R., Haghighi, H., Korsnes, R.I., Natvik, O. (2003) Chalk–fluid interactions with glycol and brines. Tectonophysics, 370, pp. 213-226

Risnes, R., Madland, M.V., Hole M., Kwabiah, N.K. (2005) Water weakening of chalk—mechanical effects of water–glycol mixtures**.** J. Pet. Sci. Eng., 48, pp. 21-36

Rutter, E. (1983) Pressure solution in nature, theory and experiment**.** J. Geophys. Soc. Lond., 140, pp. 725-740

Shiraki, R., Rock, P., Casey, W. (2000) Dissolution kinetics of calcite in 0.1 m NaCl solution at room temperature : an atomic force microscopic AFM study**.** Aquat. Geochem., 6, pp. 87-108

Swarbrick, R., Osborne, M. (1998) Mechanisms that generate abnormal pressures: an overview. B.E. Law, G.F. Ulmishek, V.I. Slavin (Eds.), Abnormal Pressures in Hydrocarbon Environments: AAPG Memoir 70, pp. 13-34

Tada, R., Siever, R. (1989) Pressure solution during diagenesis**.** Annu. Rev. Earth Planet. Sci., 17, pp. 89-118

Teufel, L.W., Rhett, D.W., (1992). Failure of chalk during waterflooding of the ekofisk field. Presented at the 1992 67th SPE Annual Technical Conference and Exhibition, Washington, DC, SPE 24911.

Weyl, P.K. (1959) **P**ressure solution and the force of crystallization—a phenomenalogical theory. J. Geophys. Res., 64, pp. 2001-2025

Xu, M., Xu, X., Knauss, K., Higgins, S. (2010) Dissolution kinetics of calcite at 50–70 °C: an atomic force microscopic study under near-equilibrium conditions. Geochem. Acta, 74, pp. 4285-4297

Yasuhara, H., Marone, C., Elsworth, D. (2005) Fault zone restrengthening and frictional healing: the role of pressure solution. J. Geophys. Res., 110, p. B06310

Zangiabadi, B., Korsnes, R.I., Hildebrand-Habel, T., Hiorth, A., Surtarjana, I.K., Lian, A., Madland, M.V. (2009) Chemical water weakening of various outcrop chalks at elevated temperature. H.I. Ling, A. Singth, R. Betti (Eds.), Poro-Mechanics IV, Destech Publications, Inc., Lancaster